Knock-sideways by inducible ER retrieval enables a novel approach for studying *Plasmodium* secreted proteins

Manuel A Fierro[1], Tahir Hussain[1], Liam J Campin[2] and Josh R Beck[1,2*]

[1]Department of Biomedical Sciences, Iowa State University, Ames, IA, 50011, USA

[2]Roy J. Carver Department of Biochemistry, Biophysics and Molecular Biology, Iowa State University, Ames, IA, 50011, USA

[*]Corresponding author: jrbeck@iastate.edu

Classification: Biological Sciences, Microbiology

Key words: *Plasmodium,* ER, ClpB1, PTEX, knock-sideways

Abstract

Malaria parasites uniquely depend on protein secretion for their obligate intracellular lifestyle but approaches for dissecting *Plasmodium* secreted protein functions are limited. We report knockER, a novel DiCre-mediated knock-sideways approach to sequester secreted proteins in the ER by inducible fusion with a KDEL ER-retrieval sequence. We show conditional ER sequestration of diverse proteins is not generally toxic, enabling loss-of-function studies. We employed knockER in multiple *Plasmodium* species to interrogate the trafficking, topology and function of an assortment of proteins that traverse the secretory pathway to diverse compartments including the apicoplast (ClpB1), rhoptries (RON6), dense granules and parasitophorous vacuole (EXP2, PTEX150, HSP101). Taking advantage of the unique ability to redistribute secreted proteins from their terminal destination to the ER, we reveal vacuolar levels of the PTEX translocon component HSP101 but not PTEX150 are maintained in excess of what is required to sustain effector protein export into the erythrocyte. Intriguingly, vacuole depletion of HSP101 hypersensitized parasites to a destabilization tag that inhibits HSP101-PTEX complex formation but not to translational knockdown of the entire HSP101 pool, illustrating how redistribution of a target protein by knockER can be used to query function in a compartment-specific manner. Collectively, our results establish knockER as a novel tool for dissecting secreted protein function with sub-compartmental resolution that should be widely amenable to genetically tractable eukaryotes.

40 **Significance**

41 Protein trafficking and secretion through the endomembrane system is a defining feature of
42 eukaryotes. The secretory pathway is central to the unique biology and pathology of the obligate
43 intracellular malaria parasite, however tools for studying secreted protein function are limited.
44 Knock-sideways is a powerful mutagenesis strategy that conditionally sequesters a protein away
45 from its site of function but is generally not applicable to secreted proteins. We developed a simple
46 approach to conditionally sequester *Plasmodium* secreted proteins in the ER by inducible C-
47 terminal fusion with a KDEL ER-retrieval sequence that can be used for trafficking, topology and
48 loss-of-function studies. The knockER strategy is broadly applicable to functional dissection of
49 proteins that traverse the eukaryotic secretory pathway.

50 **Introduction**

51 Protein secretion is a fundamental biological process of all living cells. In eukaryotes this
52 is accomplished by a dedicated secretory pathway that begins with import into the Endoplasmic
53 Reticulum (ER) for initial folding and post-translational modification, followed by sorting in the
54 Golgi and post-Golgi compartments. As an obligate intracellular parasite, secreted proteins play
55 a critical role in the biology of the malaria parasite, *Plasmodium*. Through the secretory pathway,
56 proteins are trafficked into both the plasma membrane and several organelles, including a relict
57 plastid called the apicoplast that is critical for parasite metabolism (1, 2). During schizogony,
58 another subset of proteins is packaged into several distinct secretory organelles that are
59 subsequently discharged to facilitate host cell attachment and penetration (3). Invagination of the
60 host membrane by the parasite during invasion generates an intracellular microenvironment
61 called the parasitophorous vacuole (PV) which forms the interface for host-parasite interactions
62 (4). Resident PV proteins secreted into the vacuole perform critical functions at this interface,
63 including nutrient/waste exchange and protein export (5). The latter process enables parasites to
64 deploy a battery of secreted effector proteins across the PV membrane (PVM) and into the host
65 compartment, dramatically remodeling the erythrocyte to meet nutritional demands and avoid host
66 defenses (6, 7). Remarkably, it is estimated that up to 10% of the parasite genome is devoted to
67 encoding exported effectors, further highlighting the central importance of protein secretion to this
68 parasitic lifestyle (8-12).

69 As with other eukaryotes, entry into the malaria parasite secretory pathway generally
70 begins with co-translational import of proteins containing a signal peptide or transmembrane
71 domain(s) into the ER via the Sec61 complex, followed by sorting from the Golgi to internal
72 compartments, the PV or beyond into the host (13). ER-resident proteins that escape the ER via
73 bulk flow in COPII vesicles are returned to the ER in COPI vesicles by ERD2 surveillance, which
74 binds a C-terminal retrieval sequence ("KDEL" and variants) in the *cis* Golgi and releases it in the
75 ER in a pH-dependent manner (14-16). Similar to other eukaryotes, ER retention of secreted

76 reporters or chimeric proteins can be achieved in *Plasmodium spp.* by a C-terminal KDEL or
77 functional variants (17-22).

78 In this present work, we developed and characterized a novel DiCre-based knock-
79 sideways tool called knockER that enables conditional fusion of KDEL to the C-terminus of
80 secreted proteins, subjecting the target protein to ERD2 surveillance in the *cis* Golgi to cause its
81 retrieval to the ER. Using this approach, we show successful conditional retrieval of five
82 endogenous *Plasmodium* proteins (ClpB1, RON6, EXP2, PTEX150 and HSP101) that traffic
83 through the ER to diverse compartments including the apicoplast, rhoptries, dense granules, and
84 the PV. Importantly, conditional ER retrieval of both highly expressed reporters and endogenously
85 tagged proteins does not generally impact fitness, indicating knockER-mediated phenotypes are
86 not the indirect result of an integrated stress response, thus making this system suitable for protein
87 loss-of-function studies. Taking advantage of the unique ability to redistribute secreted proteins
88 from their terminal destination to the ER, we reveal a surprising indifference to ER retrieval of
89 HSP101 in *P. falciparum*, in contrast to the other PTEX components, indicating HSP101 is
90 maintained in excess in the PV. Interestingly, redistribution of HSP101 from the PV to the ER
91 hypersensitized parasites to a post-translational destabilization tag that disrupts HSP101
92 interaction with PTEX but not to translational knockdown, providing support for an HSP101
93 function in the early secretory pathway in addition to its role in protein translocation across the
94 PVM in the assembled PTEX complex, as recently proposed (23-25). These results establish
95 knockER as a novel tool to study eukaryotic secreted proteins.

96

97 **Results**

98 **Conditional ER retrieval of a secreted reporter does not impact parasite fitness**

99 To facilitate conditional ER retrieval of a protein of interest, we designed a strategy based
100 on the dimerizable Cre recombinase (DiCre) system (26, 27) where a gene of interest is C-
101 terminally fused to a 3xFLAG tag and a stop codon flanked by *loxP* sequences imbedded in small

102 introns (28). Activation of DiCre by rapamycin results in excision of the loxP-intervening sequence,
103 removing the 3xFLAG tag and stop codon and bringing into frame a 3xHA tag followed by the ER-
104 retention sequence KDEL and a stop codon (Figure 1A). While the ER plays a crucial role in
105 quality control and is sensitive to added stress, several previous studies have exogenously
106 expressed various KDEL or SDEL fusion proteins in *P. falciparum* and *P. berghei* without apparent
107 impact on parasite fitness (19, 29-36). To directly ascertain whether ER retrieval of a highly
108 expressed secreted protein impacted parasite fitness, we first appended the knockER system to
109 an mNeonGreen (mNG) reporter and fused this to the *exp2* 5' UTR and signal peptide, enabling
110 expression from the strong *exp2* promoter and entry into the ER followed by default secretion into
111 the PV (37-39). This assembly was placed under control of the anhydrotetracycline (aTc)-
112 responsive TetR-DOZI-aptamers system to prevent expression until aTc is present in the culture
113 (Figure 1A) (40, 41). To combine the Bxb1 integrase system with DiCre, we first introduced a
114 DiCre expression cassette at the benign *pfs47* locus (27) in the *P. falciparum* NF54^{attB} strain (42)
115 (Figure S1) and then integrated the mNG-knockER reporter construct at the *attB* site in the *cg6*
116 locus on chromosome 6 in this NF54$^{attB\text{-}DiCre}$ line.

117 Upon treatment with 10nM rapamycin for 3 hours, parasites efficiently excised the
118 knockER cassette (kER) with essentially complete conversion of the population within one
119 parasite developmental cycle (48 hrs) resulting in the expected tag switching from FLAG to HA
120 (Figure 1B,C). Examination of DMSO vehicle-treated parasites by live microscopy showed a
121 peripheral mNG signal, consistent with secretion to the PV (Figure 1D). In contrast, following
122 treatment with rapamycin the mNG signal was dramatically altered to an intracellular, perinuclear
123 pattern that co-localized with ER Tracker, confirming retention in the ER (Figure 1D).
124 Quantification of the distribution of mNG fluorescence between the parasite periphery and interior
125 showed substantial, stable re-localization following KDEL fusion, indicating robust retrieval by
126 ERD2 (Figure 1E, mean % internal mNG at 24hrs: 48.78 ± 5.8% in DMSO vs 76.87 ± 8.9% in
127 Rap, and at 168hrs: 42.54 ± 6.0% in DMSO vs 84.66 ± 6.9% in Rap). Importantly, ER retention

128 of mNG had no impact on parasite growth (Figure 1F) showing that knockER can successfully
129 retrieve a secreted reporter to the ER without impacting parasite fitness.
130
131 **knockER reveals Golgi-dependent trafficking and essential apicoplast functionality of**
132 **ClpB1**
133 Next, we applied knockER to an endogenous gene for conditional loss-of-function
134 mutagenesis. We choose ClpB1, a poorly characterized, nuclear-encoded AAA+ class 1
135 Clp/HSP100 chaperone that is targeted to the apicoplast (43). As apicoplast ablation can be
136 chemically rescued with isopentenyl pyrophosphate (IPP) (44), we reasoned that IPP
137 supplementation would provide a simple validation that any loss of parasite fitness is a direct
138 effect of sequestering ClpB1 away from its site of action and not an indirect result of ER stress.
139 ClpB1 contains both a signal peptide for ER entry and a transit peptide for apicoplast targeting
140 and localization of ClpB1 to this organelle was previously confirmed by both microscopy and
141 proteomic analyses (35, 43). Using CRISPR/Cas9 editing, we fused mNG to the C-terminus of
142 ClpB1 followed by the kER cassette (Figure 2A). As expected, IFA demonstrated co-localization
143 with the apicoplast marker ACP1, confirming ClpB1 localization to this organelle (Figure 2B).
144 Treatment with rapamycin resulted in efficient excision (Figure 2C) and switching to the 3xHA-
145 KDEL tag produced a shift in migration by Western blot consistent with an increase in molecular
146 weight of ~14 kDa in the rapamycin treated samples, indicating that the N-terminal transit peptide
147 (residues 24-152, 13.9 kDa) is no longer cleaved in the ClpB1-KDEL fusion (Figure 2D). Since
148 this maturation event takes place in the apicoplast (45), this suggested that ClpB1 was no longer
149 being trafficked to this organelle. Indeed, live microscopy showed a dramatic re-localization of
150 mNG from puncta to a perinuclear distribution that co-localized with ER Tracker, indicative of
151 successful ER retrieval (Figure 2E).
152 While its functional importance has not been directly tested, ClpB1 is expected to be
153 essential for blood-stage survival based on saturating insertional mutagenesis in *P. falciparum*

154 and pooled knockout screens in *P. berghei* (46, 47). Indeed, ER retention of ClpB1 was lethal and
155 resulted in delayed parasite death (Figure 2F), consistent with an essential role in the apicoplast
156 (48, 49). Moreover, supplementation with IPP fully rescued parasite growth, confirming the
157 observed phenotype was apicoplast-specific and not due to a disruption of ER homeostasis
158 following ClpB1 retention (Figure 2F). Rapamycin-treated parasites supplemented with IPP
159 showed dispersed, vesicular ACP1 signal consistent with plastid disruption, further indicating
160 ClpB1 is required for apicoplast maintenance (Figure 2G). Taken together, these results show for
161 the first time that ClpB1 is an indispensable component of the apicoplast machinery and illustrate
162 that knockER can be used for protein loss-of-function studies in *P. falciparum*.
163
164 **knockER induces ER retrieval of rhoptry proteins**
165 Having demonstrated that knockER is suitable to generate loss-of-function phenotypes by
166 protein mis-localization to the ER, we next tested this knock-sideways approach on an expanded
167 set of endogenous soluble and membrane proteins that traffic through the secretory pathway to
168 diverse destinations, including secretory organelles and the PV/PVM. We began by attempting to
169 retrieve RON6, a soluble rhoptry-neck protein that is injected into the PV during invasion (Figure
170 S2A,B). Attempts predating CRISPR technology to disrupt *Pfron6* or truncate its Cysteine-rich C-
171 terminus were unsuccessful (50). More recently, saturating transposon mutagenesis in *P.*
172 *falciparum* recovered a single insertion within an intron (46) expected to generate a truncation at
173 residue 713 of 950, leaving most of the protein intact (Figure S2A). Curiously, RON6 orthologs in
174 rodent malaria parasites lack the cysteine-rich region which accounts for the C-terminal ~23% of
175 *P. falciparum* RON6, roughly corresponding to the truncated region in the insertional mutant. As
176 RON6 was not targeted in the PlasmoGEM data set, its suspected essentiality remains uncertain
177 (47). To directly test the importance of RON6, we generated RON6-kER parasites, which
178 underwent efficient excision upon rapamycin treatment (Figure S2C,D). Rapamycin treatment
179 resulted in re-localization of RON6-mNG from the rhoptries to the ER and produced a minor but

180 reproducible growth defect (Figure S2D-F). These results suggest that RON6 may be dispensable
181 in the blood stage, although we cannot exclude the possibility that small amounts of RON6-KDEL
182 may escape ERD2 surveillance at levels sufficient to mediate a critical function. Additionally, the
183 minor fitness defect that results from RON6-KDEL fusion could be the indirect result of modest
184 ER stress induced by RON6 retention. Nonetheless, these findings clearly demonstrate that
185 knockER efficiently retrieves secretory proteins synthesized during the brief period of merozoite
186 formation at the terminal phase of intraerythrocytic development.
187

188 **ER retention of EXP2 produces a lethal defect independent to loss of PVM transport**
189 **function**

190 Having successfully retained several soluble proteins in the ER using knockER, we next
191 tested conditional retrieval of a membrane protein. Solute permeation across the PVM is mediated
192 by a nutrient-permeable channel (51, 52) whose identity was recently tied to EXP2, a PVM protein
193 broadly conserved among vacuole-dwelling apicomplexans (53, 54). EXP2 contains a signal
194 peptide followed by an N-terminal amphipathic helix and oligomerizes to form a heptameric pore
195 in the PVM (25, 55, 56). It is currently unknown how pore formation is specifically constrained to
196 the PVM to avoid perforating other membranes along the secretory pathway or the parasite
197 plasma membrane. While not structurally homologous to the EXP2 pore, bacterial α-helical pore
198 forming toxins are functionally analogous and provide a possible model for EXP2 pore formation.
199 These proteins are typically maintained in a monomeric state that shields a membrane-spanning
200 amphipathic helix, enabling soluble trafficking until contact with components of a target membrane
201 triggers conformational rearrangement, leading to membrane insertion and oligomerization (57).

202 If EXP2 traffics in a similar configuration, then its C-terminus will enter the secretory
203 pathway lumen and be sensitive to ER-retrieval by KDEL fusion. Indeed, we endogenously tagged
204 EXP2 with a version of the kER cassette lacking mNG and found that KDEL fusion disrupted
205 EXP2 trafficking to the PV and resulted in ER retention, confirming its C-terminus resides in the

206 secretory pathway lumen (Figure 3A-D). Notably, ER retrieval of EXP2 appeared to cause more
207 rapid parasite death than previously observed by conditional knockdown or knockout approaches
208 (53, 58, 59) (Figure 3E). To confirm this observation, we engineered parasites to enable DiCre-
209 mediated conditional knockout of EXP2 (EXP2-cKO) to allow for matched induction kinetics to
210 EXP2-kER (Figure S3A-C). Following activation of DiCre in synchronized, ring-stage parasites,
211 the EXP2 knockout progressed to the next cycle with equivalent new ring parasitemia to the
212 DMSO control before death in the second cycle; in contrast, EXP2-kER parasites died
213 immediately in the first cycle and did not form new rings (Figure S3D). To test whether parasite
214 death was solely due to loss of EXP2 transport functions in the PV and not an indirect result of
215 retaining EXP2 in the ER, we generated parasites expressing a second copy of EXP2-mNG-kER
216 from the *attB* locus under the control of its own promoter, leaving the endogenous EXP2 locus
217 unaltered (Figure S3E-G). Retrieval of this second copy of EXP2 to the ER also resulted in
218 parasite death, indicating that EXP2 retention in the ER is toxic independent of compromised
219 transport functions at the PVM (Figure 3F,G). In contrast, ER retrieval of a second copy of EXP2
220 lacking the amphipathic helix did not cause parasite death (Figure 3H,I and S3E-G). As expected,
221 prior to KDEL fusion the ΔTM version of EXP2 localized to the PV and the digestive vacuole (due
222 to endocytosis of PV proteins along with RBC cytosol). Surprisingly, most cells also showed
223 EXP2ΔTM-mNG export into the RBC cytoplasm (arrow, Figure 3H and S3H). The basis for
224 EXP2ΔTM-mNG export is unclear but may result from interactions with other PTEX components
225 that somehow result in recognition as cargo in the absence of the amphipathic helix. The
226 requirement for the amphipathic helix in EXP2-kER toxicity suggests that increasing EXP2 dwell
227 time in the early secretory pathway may trigger an unfolded protein response or cause aberrant
228 EXP2 pore formation in the ER membrane. Thus, this may provide a new tool for studying EXP2
229 pore formation but also indicates knockER may not be appropriate for loss-of-function studies of
230 certain membrane proteins.
231

232 **ER retention of PTEX150 but not HSP101 results in loss of PTEX function in *P. falciparum***

233 In malaria parasites, the nutrient-permeable channel has been additionally functionalized
234 by the flange-like adaptor PTEX150 which docks the AAA+ chaperone HSP101 onto EXP2 to
235 form the *Plasmodium* Translocon of Exported proteins (PTEX), transforming EXP2 into a protein-
236 conducting pore to translocate effector proteins across the PVM and into the erythrocyte (23-25,
237 53, 60). Interestingly, HSP101 shows a dual localization to both the PV and the ER as opposed
238 to EXP2 and PTEX150, which localize exclusively to the PV and form a sub-complex independent
239 of HSP101 (34, 39, 61, 62). We verified this unique ER localization of HSP101 by protease
240 protection assays in parasite lines expressing fluorescently tagged versions of each PTEX core
241 component, confirming an internal, perinuclear pool of HSP101 but not EXP2 or PTEX150 (Figure
242 S4). This arrangement suggests that in addition to powering translocation in the assembled PTEX
243 complex, HSP101 may also function upstream of the vacuole, possibly initiating cargo selection
244 early in the secretory pathway (61). While several HSP101 conditional knockdown (24, 61) or
245 inactivation (23) strategies have demonstrated an essential role in protein export, it is difficult to
246 resolve distinct compartmental functions with these mutants given that they impact the total
247 protein pool and have no sub-compartmental resolution. In contrast, knockER can potentially
248 resolve functions across distinct compartments by redistributing a target protein pool from its
249 terminal destination to the ER.

250 In an attempt to separate HSP101 ER function from its role in the PV, we generated a kER
251 fusion to the endogenous copy of HSP101, expecting that redistribution of HSP101 to the ER
252 would be lethal but might provide insight into any ER localized function which could be preserved
253 compared to the phenotype of HSP101 knockdown mutants. In parallel, we also generated a
254 PTEX150-kER line, reasoning that since HSP101 and PTEX150 have similar expression timing
255 and are exclusively involved in protein export but not nutrient uptake (53), PTEX150 would provide
256 a control for knockER inactivation of PTEX activity independent of ER function. As expected, the
257 PTEX150-KDEL fusion was efficiently retrieved to the ER, producing a lethal growth defect and

258 accompanying block in protein export (Figure 4A-E), similar to *glmS* ribozyme-mediated
259 knockdown of PTEX150 (24). Importantly, ER retention of a second copy of PTEX150-kER in
260 parasites where the endogenous PTEX150 locus was unmodified did not impact growth,
261 demonstrating that the phenotype observed upon ER retention of the endogenously tagged
262 protein is a direct result of functional disruption of PTEX150 (Figure S5A-D).

263 Unexpectedly, although rapamycin-induced HSP101-KDEL fusion increased ER
264 localization similar to PTEX150 (Figure 4F-H), parasite growth was completely unaffected and
265 protein export was not detectibly impacted (Figure 4I,J), sharply contrasting with the lethal export
266 defect observed with HSP101 depletion or inactivation mutants (23, 24, 61). Indeed, HSP101-
267 kER parasites could be cultured indefinitely following excision and displayed sustained ER
268 retention of HSP101 (Figure 4H and S5E,F, mean Rap internal HSP101: 58.82±9.58% at 24 hours
269 vs 54.82±9.84% at 7 days). As an orthogonal approach to monitor protein redistribution by KDEL
270 fusion, we released infected RBCs with saponin to permeabilize the PVM and quantified
271 fluorescence via flow cytometry with or without proteinase K treatment. Again, we observed an
272 increase in protected fluorescence following rapamycin treatment, consistent with redistribution
273 of HSP101 to the ER (Figure S5G). Importantly, PCR and Western blot indicated that rapamycin-
274 treated parasites had undergone complete excision with the pre-excised FLAG-tagged version of
275 HSP101 no longer detectible (Figure 4F,G). Furthermore, both the mNG-FLAG and mNG-HA-
276 KDEL tagged versions of HSP101 migrated as a single band at the expected size for the full-
277 length fusion proteins with no apparent breakdown products, ensuring that the mNG signal
278 distribution observed by live microscopy reflected an intact HSP101 fusion (Figure 4G, S7B and
279 S8B).

280 While a large fraction of PTEX150 and HSP101 was clearly ER-retained following
281 knockER induction, some peripheral signal was still apparent after rapamycin treatment (Figure
282 4C,H). To determine whether the observed phenotypic differences between HSP101 and

283 PTEX150 were due to a difference in sensitivity to ERD2 surveillance, we quantified the internal
284 mNG fluorescence signal in HSP101- and PTEX150-kER parasites following KDEL fusion. In
285 synchronized parasites, a similar increase in internal signal was observed in both lines at 24 hours
286 post Rap treatment (Figure S5E, mean Rap internal HSP101 58.82±9.58% vs 56.32±18.56% for
287 PTEX150). Since a comparison could not be made with PTEX150-kER parasites at 7 days due
288 to parasite death by the second cycle following excision, we compared HSP101-kER parasites
289 with second copy PTEX150-kER^{attB} control parasites 7 days after excision and again observed a
290 comparable internal signal redistribution (Figure S5F, mean Rap internal HSP101 54.82±9.84%
291 vs 61.75±16.27% for PTEX150 at 7 days). As major differences in ER retrieval cannot account
292 for parasite insensitivity to HSP101-kER, these results indicate vacuolar HSP101 levels are
293 unexpectedly maintained in excess from what is required for PTEX function at the PVM.
294

295 **ER retention of *P. berghei* HSP101 results in a lethal export defect**

296 To determine if ER retention of HSP101 was similarly tolerated in other *Plasmodium*
297 species, we tagged HSP101 and PTEX150 with kER in a *P. berghei* rodent malaria DiCre
298 parasite. We also included a downstream cassette in this tagging plasmid for expression of a
299 secreted mRuby under control of the constitutive *Pbhsp70* promoter to label the PV (Figure S6A).
300 Similar to *P. falciparum* knockER mutants, rapamycin treatment produced efficient excision and
301 ER retrieval of PbPTEX150 and PbHSP101 (Figure 5A-C,F). Curiously, the localization pattern of
302 KDEL fusion proteins in *P. berghei* parasites was clearly internal to PV-mRuby but more diffuse
303 than in *P. falciparum*, suggesting distinctive ER morphology between these two species.
304 Interestingly, PbHSP101-kER and PbPTEX150-kER parasites displayed greater internal retention
305 than the corresponding *P. falciparum* knockER mutants (HSP101: mean % internal mNG 77.42 ±
306 7.72% in *P. berghei* vs 58.82±9.58% in *P. falciparum*; and PTEX150: mean % internal mNG 69.55
307 ± 10.86% in *P. berghei* vs 56.32±18.56% in *P. falciparum*), suggesting that KDEL-mediated ER

308 retrieval is more stringent in rodent parasites (Figure 5D,G). To evaluate protein export, we
309 generated versions of the PbPTEX150-kER and PbHSP101-kER mutants where the PV-mRuby
310 reporter was replaced with a cassette for expression of the exported protein IBIS1 fused to mRuby
311 (Figure S6A) (63). In contrast to *P. falciparum*, KDEL fusion to both PbPTEX150 and PbHSP101
312 produced a stark block in IBIS1 export (Figure 5I,J). To determine if KDEL fusion to PbHSP101
313 impacted parasite fitness, parasites were induced *ex vivo* followed by overnight culture to allow
314 for tag switching before equal numbers of DMSO or rapamycin treated parasites were IV injected
315 into naïve mice. Strikingly, while DMSO controls became patent by day two post-injection, neither
316 KDEL-fused PbPTEX150 or PbHSP101 parasites appeared over the course of 10 days before
317 the experiment was terminated (Figure 5E,H and S6B).

318 The block in IBIS1 export suggests that PbHSP101-KDEL is sufficiently retained to
319 produce a lethal export defect, in contrast with PfHSP101-KDEL; however, phenotypes can be
320 masked by the rich resources available in culture (64, 65) and many exported effectors critical for
321 survival in the vertebrate host are dispensable *in vitro* (12) where parasites do not have to contend
322 with host defenses (66, 67). To distinguish whether the fitness defect incurred by ER retention of
323 PbHSP101 resulted simply from parasite death or from the unique pressures imposed by the host,
324 we evaluated parasite development of synchronized ring-stage cultures *ex vivo*. Importantly, both
325 PbHSP101-kER and PbPTEX150-kER parasites also failed to develop into terminal schizonts *in*
326 *vitro* following rapamycin treatment, indicating the *in vivo* fitness defect is not merely the result of
327 host defenses (Figure S6C-E). Taken together, our data show that ER-retention of HSP101-KDEL
328 is more efficient in *P. berghei,* resulting in a lethal defect in protein export.

329

330 **ER retention of HSP101 hypersensitizes parasites to a destabilization tag that inhibits**
331 **HSP101-PTEX complex formation**

332 The lack of an observable phenotype after ER-retention of HSP101 in *P. falciparum*
333 suggests that the level of retention does not reach a critical threshold required to impact HSP101

334 function at the PV. To determine the amount of HSP101 needed to support *P. falciparum* growth
335 *in vitro*, we combined knockER with the TetR-DOZI-aptamers system to generate a HSP101-kER
336 line that also allows for titration of HSP101 expression with aTc (Figure 6A). Like the original
337 HSP101-kER line, rapamycin-treated HSP101-kER$^{TetR\text{-}DOZI}$ parasites exhibited ER retention of
338 HSP101 without impacting parasite growth or export of representative PEXEL and PNEP proteins
339 (Figure 6B-D). However, HSP101 depletion following aTc washout resulted in a robust block in
340 protein export and parasite death (Figure 6D and S7A,B), consistent with previous HSP101
341 knockdown or inactivation studies (23, 24, 61). To determine the level of total HSP101 reduction
342 sufficient to impact growth, we grew synchronized parasites at a range of aTc concentrations
343 following DMSO or rapamycin treatment and measured mNG fluorescence via flow cytometry in
344 parallel with parasite growth (Figure 6E,F). Interestingly, rapamycin-treated parasites grown at
345 higher aTc concentrations displayed a small but reproducible increase in total HSP101, consistent
346 with a reduction in HSP101 turnover by endocytosis from the PV to the digestive vacuole following
347 redistribution to the ER (Figure 6E). More importantly, we determined that a ~70% reduction in
348 total HSP101 levels was necessary to impact parasite growth, showing that a relatively small
349 amount of HSP101 is needed for survival (Figure 6E,F, 5nM aTc), consistent with redistribution
350 of HSP101 by knockER not meeting the threshold required to impact HSP101 PV function and
351 parasite fitness in *P. falciparum*.

352 If HSP101 functions exclusively in the PV, then knockER-mediated depletion of vacuolar
353 HSP101 levels should hypersensitize parasites to HSP101 knockdown. However, dose-response
354 to aTc was unaltered by rapamycin-treatment (Figure 6G) and the growth defect of KDEL-fused
355 HSP101 parasites maintained at 5 nM aTc was indistinguishable from the DMSO control even
356 over an extended 10-day growth assay (Figure 6F), possibly suggesting that the PV-localized
357 function of HSP101 may not fully account for its role in parasite fitness. To ensure depletion of
358 HSP101 from the vacuole by knockER sensitizes parasites to compromised HSP101 PV function,
359 we generated an HSP101-knockER line where mNG was replaced by a ligand-sensitive DHFR-

360 based destabilization domain (DDD) (Figure 6H) (23). In the absence of trimethoprim (TMP), the
361 DDD blocks HSP101 interaction with EXP2/PTEX150 but not cargo binding, specifically targeting
362 function of the assembled PTEX complex in the PV (23). In contrast to translational knockdown,
363 HSP101-kER^{DDD} parasites were hypersensitized to reduction of TMP levels following rapamycin-
364 treatment, indicating a synergistic effect when the reduction of HSP101 PV levels is combined
365 with disruption of PTEX complex formation (Figure 6I and S7C-E). Taken together, these results
366 illustrate how knockER can be used to study protein function with sub compartmental resolution
367 and may support a distinct HSP101 activity in the ER upstream of its PVM translocation function
368 at the assembled PTEX complex.
369

370 **Discussion**

371 Several genetic tools are now available for protein loss-of-function studies in *Plasmodium*
372 *spp.* (68), including knock-sideways for conditional sequestration of a target protein away from its
373 normal site of function (69, 70). While this system is not currently amenable to parasite proteins
374 that enter the secretory pathway, conditional control of secretory traffic has been achieved in *P.*
375 *falciparum* by ligand-mediated alteration of the N-terminal transit peptide that controls apicoplast
376 targeting, enabling redirection of plastid proteins into the default secretory pathway (71).
377 Additionally, conditional ER release systems have been developed in model eukaryotes based
378 on ER retrieval machinery (72). In contrast, knockER provides a simple, DiCre-mediated knock-
379 sideways strategy that exploits the ERD2/KDEL receptor (KDELR) system for conditional ER
380 retrieval, providing a generalizable approach for interrogating secreted proteins in genetically
381 tractable eukaryotes.

382 In this study, we demonstrate knockER simultaneously allows for trafficking and loss-of-
383 function studies. The ability to determine whether a protein traffics from the ER through the *cis*
384 Golgi is an important consideration for nuclear-encoded apicoplast proteins since Golgi-
385 dependent and -independent trafficking routes have been reported (31, 33, 73). While these

386 apicoplast trafficking studies were carried out with reporters and chimeras, knockER allows for
387 monitoring *cis* Golgi transit of endogenous proteins. The sensitivity of ClpB1 to KDEL-mediated
388 ER retrieval demonstrates a Golgi-dependent trafficking route to the apicoplast. Moreover, we
389 show for the first time that this AAA+ chaperone is essential for apicoplast maintenance. ClpB1 is
390 one of four Clp/HSP100 chaperones encoded by *Plasmodium spp*., three of which localize to the
391 parasite plastid while the fourth, HSP101 (previously known as ClpB2) localizes to the PV and
392 ER (43). The other apicoplast-targeted members of this quartet include the nuclear-encoded
393 ClpC, which mediates regulated proteolysis together with the serine protease ClpP (74, 75), and
394 ClpM, now the only uncharacterized member of this group and one of the few proteins encoded
395 on the apicoplast genome. Similar to the well-studied function of its closest orthologs (76), ClpB1
396 likely acts as a disaggregase that, together with ClpC/P and ClpM, forms a critical proteostasis
397 system required to maintain and regulate the apicoplast proteome (77).

398 ER perturbations can trigger an integrated stress response leading to cell arrest or death
399 (78, 79). *Plasmodium* possesses one of the widely conserved ER stress sensors, the PERK-
400 eIF2α pathway which halts protein translation and flux through the secretory pathway (20, 80-83).
401 Importantly, conditional ER retrieval of proteins produced from their endogenous locus or by
402 heterologous expression was not generally toxic, enabling loss-of-function studies with knockER.
403 The single notable exception was EXP2, which rapidly killed parasites when retained in the ER
404 independent to loss of its PVM transport function, indicating knockER experiments should be
405 controlled for indirect effects. EXP2-KDEL toxicity was dependent on the amphipathic helix that
406 forms the membrane-spanning region in the oligomeric EXP2 pore (25), suggesting that
407 accumulation of EXP2 in the ER might trigger an unfolded protein response or lead to premature
408 pore formation in the early secretory pathway. More work is required to determine if this outcome
409 is specific to EXP2 but the observation that parasites tolerate SDEL-mediated retention of several
410 TM domain-containing exported proteins indicates this is not a general problem for unnatural ER-
411 retrieval of membrane proteins (84). Indirect fitness defects aside, retrieval of EXP2-KDEL

412 demonstrates that its C-terminus enters the secretory pathway lumen, consistent with a soluble
413 EXP2 trafficking state that precedes membrane integration at the PVM. Regardless of the basis
414 for EXP2-kER toxicity, these experiments highlight that knockER can also be used to investigate
415 membrane topology. While ER-resident type I membrane proteins utilize a different mechanism
416 for retrieval as their C-termini face the cytosol of the cell (85, 86), ERD2/KDELR can retrieve
417 membrane proteins whose C-termini face the lumen (87) and thus knockER should be able to
418 distinguish the topology of single and multi-pass transmembrane domain-containing proteins.

419 A unique feature of knockER is the ability to redistribute secreted proteins from their
420 terminal destination to the ER. We tagged both HSP101 and the translocon adaptor PTEX150
421 with knockER, reasoning that ER retrieval of either protein would produce a lethal export defect
422 but that differential impacts on exported cargo trafficking might be exposed. Unexpectedly, ER
423 retrieval of HSP101 had no impact on *P. falciparum* growth or export of representative PEXEL
424 and PNEP proteins *in vitro*. Similar PV depletion of PTEX150 produced the anticipated lethal
425 export block, revealing that HSP101 PV levels are uniquely maintained in excess. As a AAA+
426 ATPase, HSP101 is the only enzyme in the PTEX core complex and its activity may exceed what
427 is required to support parasite fitness, at least during *in vitro* culture, as previously seen for the
428 aspartic protease Plasmepsin V that licenses proteins for export in the ER (88, 89). Interestingly,
429 parallel experiments in *P. berghei* resulted in greater retention and produced a lethal export defect
430 for both PTEX150 and HSP101, showing knockER is also suitable for conditional mutagenesis in
431 this important model species and suggesting retrieval may be more stringent in *P. berghei*, at
432 least for some proteins. Notably, the strength of ERD2/KDELR binding between different C-
433 terminal retrieval motifs varies by as much as 10-fold in higher eukaryotes (16). While KDEL-
434 mediated retrieval was generally robust across the diverse set of reporters and endogenous
435 proteins surveyed in *P. falciparum* and *P. berghei*, a range of functional variants have been
436 validated or can be inferred in *Plasmodium spp.* (19) and other retrieval motifs may enable tuning
437 the strength of retention by knockER.

438 Intriguingly, redistribution of HSP101 from the PV to the ER hypersensitized parasites to
439 DDD-mediated HSP101 inactivation but not translational knockdown. While TetR-DOZI
440 knockdown depletes the entire HSP101 pool, HSP101-DDD acts post-translationally by disrupting
441 complex formation with EXP2/PTEX150 but not cargo recognition (23), specifically targeting
442 HSP101 function in PVM translocation. While these results do not enable strong conclusions
443 about potential extra vacuolar activity of HSP101, they suggest that the PV-localized function may
444 not fully account for HSP101's contribution to parasite fitness, in line with a hypothesized role in
445 exported cargo recognition and/or trafficking at the ER (61). Notably, IBIS1 was not retained in
446 the ER with PbHSP101-KDEL but accumulated in the PV and was not exported into the RBC,
447 indicating that HSP101 is not required to directly chaperone cargo from the ER to the PV. Future
448 work dissecting the specific extra-vacuolar role(s) of HSP101 may resolve the long-standing
449 question of how early events in this pathway that mark proteins for export, such as PEXEL
450 processing during ER entry, are connected to cargo recognition and ultimate PVM translocation
451 into the host cell at the assembled PTEX complex.
452
453 **Materials and Methods**
454 **Parasite culture.** *P. falciparum* NF54$^{attB\text{-}DiCre}$ and derivatives were cultured in RPMI 1640 medium
455 supplemented with 27 mM sodium bicarbonate, 11 mM glucose, 0.37 mM hypoxanthine, 10 µg/ml
456 gentamicin and 0.5% Albumax I (Gibco). Parasites were maintained in deidentified, Institutional
457 Review Board-exempt RBCs obtained from the American National Red Cross. *P. berghei* ANKA
458 clone 2.34 and derivatives were maintained in Swiss Webster mice (Charles River). All
459 experiments involving rodents were reviewed and approved by the Iowa State University
460 Institutional Animal Care and Use Committee.
461
462 **Plasmids and genetic modification of *P. falciparum* and *P. berghei*.** All cloning was carried
463 out with NEBuilder HIFI DNA assembly (NEB). Primer sequences are given in Table S1. To

464 generate NF54$^{attB\text{-}DiCre}$ parasites, a DiCre expression cassette was inserted into the *pfs47* gene in
465 NF54^{attB} parasites (42) using a marker-free CRISPR/Cas9 editing strategy as described (27). Loss
466 of the endogenous *pfs47* locus was monitored with primers P1/2 and P3/4 and integration was
467 confirmed using primers P1/5 and P6/4. To confirm DiCre activity in this line, a loxP-flanked mNG
468 coding sequence with a 3xHA tag was PCR amplified using primers P19/20 and inserted between
469 AvrII and AflII in pLN-ENR-GFP cite (90), resulting in the plasmid JRB416. This plasmid was co-
470 transfected with pINT (90) into NF54$^{attB\text{-}DiCre}$ parasites and selection was applied with 2.5 µg/ml
471 blasticidin-S 24 hrs post-transfection.

472 To generate the kER fusion cassette, homology flanks targeting the 3' end of *exp2* were
473 amplified from pyPM2GT-EXP2-3xHA-GFP11 (53) using P21/22 and inserted between XhoI and
474 AvrII in pPM2GT-HSP101-3xFLAG (53). The loxPint sequence (28) was amplified with P23/24
475 and inserted immediately upstream of the 3xFLAG tag at AvrII in this vector. A partial loxPint
476 containing the loxP sequence and 3' portion of the intron followed by a 3xHA-KDEL tag was then
477 amplified with P25/26 and inserted into EagI, resulting in the plasmid JRB492. Finally, the mNG
478 coding sequencing was amplified from pyPM2GT-EXP2-mNG (91) with P27/28 and inserted into
479 AvrII in JRB492, resulting in plasmid JRB508. For generation of the *exp2* DiCre conditional
480 knockout line, a recoded version of the *exp2* coding sequence with a 3' 3xHA tag and flanked by
481 loxP sites was amplified using P76/77 from plasmid pEXP2^{apt} (53) and inserted between
482 AvrII/EagI in plasmid JRB492. A 5' flank immediately upstream of the *exp2* start codon was then
483 amplified from *P. falciparum* gDNA using P78/79 and inserted between AflII/AvrII, replacing the
484 AflII site with AscI and resulting in the plasmid JRB467. This plasmid was linearized with AscI and
485 co-transfected with pUF-Cas9-EXP2-CT-gRNA into NF54$^{attB\text{-}DiCre}$. Selection was applied with 5
486 nM WR99120 24 hrs post-transfection and clonal lines were isolated by limiting dilution after
487 parasites returned from selection.

488 To generate the SP-mNG-kER reporter, the *exp2* promoter and signal peptide were
489 amplified from parasite genomic DNA with P29/30 and the mNG-KER cassette was amplified from

490 JRB508 with P31/32 and these amplicons were assembled together in a second PCR reaction
491 with P29/32 and inserted into AscI/ApaI in pKD (41), resulting in the plasmid JRB543. For
492 expression of a second copy of EXP2-kER from the attB locus, the *exp2* promoter and full-length
493 gene were amplified from genomic DNA with P29/33 and inserted between AscI/BamHI in
494 JRB543, resulting in the plasmid JRB526. For expression of a second copy of EXP2-kER lacking
495 the amphipathic helix, a recoded portion of the *exp2* coding sequence beginning at codon 86
496 (after the amphipathic helix and immediately before the helical body domain) was amplified from
497 pEXP2^{apt} (53) and inserted at BamHI after the EXP2 signal peptide in JRB543, resulting in the
498 plasmid JRB544. These plasmids were each co-transfected with pINT and selected with 2.5 µg/ml
499 blasticidin-S as described above. To relieve translational repression by TetR-DOZI, parasite
500 cultures were supplemented with 500 nM aTc.

501 For generation of ClpB1-kER and RON6-kER lines, a Cas9 gRNA target was chosen just
502 downstream (*clpB1*, ATTTTTAGAAAAATATTATG) or just upstream (*ron6*,
503 TAATACATACAACGTACCAA) of the stop codon and the gRNA seed sequences were
504 synthesized as primers P34 and P35, respectively, and inserted into the AflII site of pAIO3 (39),
505 resulting in plasmids JRB143 and MAF22, respectively. To target the 3' end of *clpB1* or *ron6*, a 5'
506 homology flank (up to but not including the stop codon) was amplified from genomic DNA using
507 P36/37 or P38/39, incorporating synonymous shield mutations in the gRNA target sites. A 3'
508 homology flank was amplified using P40/41 or P42/43. The corresponding 5' and 3' flank
509 amplicons were assembled in a second PCR reaction using P40/37 and P42/39 and inserted
510 between XhoI/AvrII in JRB508, resulting in plasmids MAF20 and MAF27, respectively. These
511 plasmids were linearized with AflII and co-transfected with the corresponding Cas9/gRNA plasmid
512 into NF54$^{attB\text{-}DiCre}$. Selection was applied with 5 nM WR99120 24 hrs post-transfection and clonal
513 lines were isolated by limiting dilution after parasites returned from selection.

514 For generation of PTEX150-kER and HSP101-kER lines, flank assemblies targeting the
515 3' end of each gene were amplified using P44/45 from pyPM2GT-PTEX150-3xHA-GFP11 (53) or

516 P46/47 from pyPM2GT-HSP101-3xHA-GFP11 (53) and inserted between XhoI/AvrII in JRB508,
517 resulting in plasmids MAF16 and MAF17, respectively. These plasmids were linearized with AflII
518 and co-transfected with pAIO-PTEX150-CT-gRNA or pAIO-HSP101-CT-gRNA (53), selected with
519 5 nM WR99120 and cloned after parasites returned. For generation of the EXP2-kER line, plasmid
520 JRB492 (described above) was linearized and co-transfected with pUF-Cas9-EXP2-CT-gRNA
521 (53) and selected with 5 nM WR99120. For generation of HSP101-kER$^{TetR-DOZI}$ lines, flank
522 assembles were amplified using P48/49 and inserted between AscI/BamHI in JRB526 (described
523 above), resulting in plasmid MAF41. This plasmid was linearized with AflII and co-transfected with
524 pAIO-HSP101-CT-gRNA, selected with 2.5 µg/ml blasticidin-S and 500 nM aTc, and cloned after
525 parasites returned. For generation of HSP101-kER^{DDD} lines, the DDD was amplified from plasmid
526 pPM2GT-HSP101-3xFlag-DDD (53) using P70/71 and inserted between AvrII/BsrGI in MAF17,
527 replacing the mNG and resulting in plasmid MAF43. This plasmid was linearized with AflII and co-
528 transfected with pAIO-HSP101-CT-gRNA. Selection was applied with 10 µM TMP 24 hrs post-
529 transfection.

530 For expression of a second copy of PTEX150-kER from the *attB* locus, the *ptex150*
531 promoter and full-length gene were amplified from genomic DNA with P50/51 and the mNG-KER
532 cassette was amplified from JRB508 with P52/53. These amplicons were assembled together in
533 a second PCR reaction using P50/53 and inserted between ApaI/AflII in pLN-ENR-GFP (90),
534 resulting in the plasmid MAF39. This plasmid was co-transfected with pINT, selected with 2.5
535 µg/ml blasticidin-S and parasites were cloned after returning.

536 To generate the line bearing endogenous EXP2-mRuby and HSP101-mNG tags, the
537 plasmid pbEXP2-mRuby3 (92) was first linearized with AflII and co-transfected with pUF-Cas9-
538 EXP2-CT-gRNA (53) into NF54$^{attB-DiCre}$. Selection was applied with 2.5 µg/ml blasticidin-S. Next,
539 the mNG coding sequence was amplified using P54/55 and inserted between AvrII/EagI in
540 pPM2GT-HSP101-3xFLAG (53) to replace the FLAG tag with mNG, resulting in the plasmid
541 JRB325. This plasmid was linearized with AflII and co-transfected with pAIO-HSP101-CT-gRNA

542 (92) into the NF54$^{attB\text{-}DiCre}$::EXP2-mRuby parasites. Selection was applied with 5nM WR99120
543 resulting in the line NF54$^{attB\text{-}DiCre}$::EXP2-mRuby+HSP101-mNG.

544 For generation of PTEX150-kER and HSP101-kER lines in *P. berghei*, the plasmid pBAT
545 (93) was digested with MluI/XhoI and the primer P56 was used as an insert to remove the
546 intervening AvrII, SnaBI and XhoI sites from the MCS. Next, the mRuby3 coding sequence fused
547 to the PbEXP2 signal peptide was amplified with P57/58 and inserted between SwaI/BamHI,
548 replacing the GFP. The mNG-kER tagging sequence was amplified from plasmid JRB508 using
549 P59/60 and inserted between SacII/SphI, replacing the mCherry-3xMYC. Finally, 5' flanks to tag
550 *P. berghei hsp101* or *ptex150* with mNG-kER were amplified from *P. berghei* genomic DNA using
551 P61/62 or P63/64, respectively, and 3' flanks were amplified using P65/66 or P67/68, respectively.
552 The corresponding 5' and 3' flank amplicons were assembled with an intervening AflII site in a
553 second PCR reaction using P65/62 or P67/64, respectively, and inserted at SacII, resulting in
554 plasmids pPbHSP101-kER+SP-mRuby and pPbPTEX150-kER+SP-mRuby. The plasmids were
555 linearized at AflII and transfected as described (94) into the marker-free HP DiCre line (95).
556 Transfected parasites were reinjected into naïve mice and selection was applied with 0.07 mg/ml
557 pyrimethamine in drinking water provided *ad libitum* 24 hours later. After returning from selection,
558 transfected populations were cloned by limiting dilution IV injection into naïve mice to generate
559 isogenic populations designated PbHSP101-kER and PbPTEX150-kER. To monitor export with
560 an IBIS1-mRuby fusion, the *ibis1* gene and promoter were amplified from *P. berghei* gDNA using
561 P72/73 and the *mruby* cds was amplified using P74/75. These amplicons were assembled in a
562 second PCR reaction using P72/75 and inserted between PvuII/BamHI, resulting in plasmids
563 pPbHSP101-kER+IBIS1-mRuby and pPbPTEX150-kER+IBIS1-mRuby. Plasmids were
564 linearized at AflII and transfected as above.

565

566 ***P. falciparum* growth assays**. Growth assays were performed as described previously (22).
567 Briefly, parasites were treated with either DMSO or 10 nM rapamycin for 3 hrs and washed 1X.

568 Then, parasites were seeded between 0.2-1% parasitemia in triplicate and monitored every 48
569 hrs by flow cytometry on an Attune NxT (ThermoFisher) by nucleic acid staining with PBS
570 containing 0.8 µg/ml acridine orange. For IPP rescue experiments, ClpB1-kER cultures were
571 supplemented with 200 µM IPP. For kER fusions expressed from the *attB* locus, cultures were
572 supplemented with 1 µM aTc 24 hrs prior to rapamycin treatment to relieve TetR-DOZI-aptamer
573 translational repression. For HSP101-kER$^{TetR\text{-}DOZI}$ parasites, aTc was removed by washing
574 parasites 7X with 13 mL of media. 500 nM aTc was then supplemented back to control parasites.
575 As required, parasites were sub-cultured to avoid high parasite density, and relative parasitemia
576 at each time point was back-calculated based on actual parasitemia multiplied by the relevant
577 dilution factors. Data were displayed using Prism 9 (GraphPad Software).

578 For EC_{50} shift assays of HSP101-kER$^{TetR\text{-}DOZI}$ and HSP101-kER^{DDD}, asynchronous
579 parasites were treated with DMSO or rapamycin before removal of aTc or TMP. After agonist
580 washout as described above, parasites were seeded in triplicate at 0.5% parasitemia with 2-fold
581 dilutions starting from 500 nM aTc or 250 nM TMP and parasite growth was monitored after 72
582 hrs.

583

584 ***P. berghei* kER experiments.** Parasite-infected blood was collected by cardiac puncture when
585 parasitemia reached 3-4% and cultured in RPMI supplemented with 20% FBS. Cultures were
586 treated with 10 nM rapamycin or a DMSO vehicle control for 3 hours followed by a media change.
587 After 18 hours of additional culture, parasites were harvested for diagnostic PCR, live
588 fluorescence microscopy and Western blot. Equal numbers of DMSO or rapamycin-treated
589 infected RBCs (~10,000 parasites per injection) were IV injected into naïve mice and parasitemia
590 was monitored by giemsa-stained blood smear every two days.

591 For synchronized, *ex vivo* growth assays, parasites were IP injected into mice and allowed
592 to reach 2-3% parasitemia. Parasites gathered from cardiac puncture were then treated with
593 DMSO or 10nM rapamycin 3-4hrs, washed, and allowed to mature into schizonts overnight

594 without further rapamycin treatment. The mature schizonts were magnet purified and tail vein
595 injected into naïve mice treated with phenylhydrazine (1mg/mice) (Sigma, 114715) to allow
596 parasites to egress and invade new RBCs in mice. After 3 hrs to allow parasite egress and re-
597 invasion, synchronous ring-stage parasites were collected by cardiac puncture and allowed to
598 mature overnight *in vitro*. At 24 hrs post injection, parasite development was assessed in Giemsa-
599 stained smears and DNA content was evaluated by Hoechst 34580 staining (1:5,000) on an
600 Attune NxT flow cytometer. To monitor export of IBIS1-mRuby, parasites were IP injected and
601 allowed to grow to 2-3% parasitemia and imaged from tail-blood. Mice were then injected IP with
602 rapamycin (1 mg/kg) and parasites were observed again 24hrs later.
603
604 **Microscopy.** For live microscopy, *P. falciparum* parasites were treated with either DMSO or 10
605 nM rapamycin and viewed 24-48 hrs later. Hoechst (33342, Invitrogen; 1:10,000) was used to
606 visualize the nucleus by incubating with parasites 2-5 min prior to visualization. ER-Tracker Red
607 (Invitrogen; 1:1000) was used to visualize the ER by incubating with parasites 30 min at 37°C
608 prior to visualization. For constructs expressed from the *attB* locus under TetR-DOZI-aptamers
609 control, parasites were grown in 500 nM aTc for 24 hrs prior to incubation with DMSO or
610 rapamycin to allow expression. For RON6 parasites, DMSO and rapamycin-treated schizonts
611 were incubated with 50nM ML10 (obtained through BEI resources, NIAID, NIH and supplied by
612 LifeArc, Stevenage, UK: MRT-0207065 (ML10), NR-56525) for 4.5 hrs and visualized by
613 microscopy. For *P. berghei*, synchronized ring-stage parasites were isolated via cardiac puncture,
614 treated with DMSO or rapamycin for 3 hrs and allowed to develop overnight in culture before
615 visualization. For quantification of fluorescence signal, MFI was calculated using the measured
616 Integrated Density value from Fiji (96). The internal MFI was calculated using an ROI within the
617 parasite PV and subtracting that from the whole parasite MFI using an ROI outside the PV
618 boundary. The percent internal fluorescence was then calculated by dividing the internal MFI by
619 the whole parasite MFI.

620 For protease protection assays on live cells, parasites were treated with 0.03% saponin
621 (Sigma) in 1X PBS for 15 min at 4°C. Purified parasites where then washed once with 5 mL of 1X
622 PBS and once with 5 mL of digestion buffer (50 mM Tris pH 7.5, 150 mM NaCl, 1 mM $CaCl_2$) (61).
623 Parasite samples where then split into two identical tubes, one of which was treated with 20 µg/mL
624 of Proteinase K (740506.75, Macherey-Nagel), and incubated at 37°C for 15 min. Proteinase K
625 was removed and samples resuspended with digestion buffer plus protease inhibitor cocktail (Halt
626 78429, Thermo Scientific) before visualization.

627 For IFAs of the EXP2- and ClpB1-kER lines, parasites were treated with either DMSO or
628 10 nM rapamycin and fixed 24 hrs or 144 hrs later as described previously (22). For HSP101-
629 $kER^{TetR\text{-}DOZI}$ lines, parasites were synchronized with 5% sorbitol, treated with either DMSO or 10
630 nM rapamycin, grown with or without 500 nM aTc, and fixed 48 hrs later. Briefly, parasites were
631 fixed with Fixative Solution (4% paraformaldehyde, 0.0075% glutaraldehyde in PBS) for 25 min
632 at room temperature in the dark. Parasites were then permeabilized with 0.1% Triton in PBS for
633 10 minutes at room temperature while rocking. Parasites were washed 1X with PBS and then
634 blocked with 3% BSA in PBS for 1hr at room temperature. Primary antibody was applied in 3%
635 BSA solution for 1 hr at room temperature, washed 2X with PBS, followed by secondary antibody
636 incubation for 1 hr at room temperature. After 2X washes with PBS, parasites were adhered onto
637 Poly-L-lysine coated coverslips and then mounted onto slides. For parasites probed with SBP1,
638 parasites were acetone fixed as in (39). Briefly, thin smears were immersed in 100% acetone for
639 2 min. Smears were washed 1X with PBS and then blocked with 3% BSA in PBS for 1 hr at room
640 temperature. Primary antibody was applied in 3% BSA solution for 1 hr at room temperature,
641 washed 2X with PBS, followed by secondary antibody incubation for 1 hr at room temperature.
642 After 2X washes with PBS, slides were mounted with DAPI, covered with a coverslip and sealed.
643 The antibodies used for IFA were: mouse anti-HA antibody (clone 16B12, BioLegend; 1:200),
644 rabbit polyclonal anti-HA SG77 (ThermoFisher; 1:500), rabbit anti-PfGRP78 (BiP) (MRA-1246,
645 BEI Resources, NIAID, NIH; 1:100), mouse monoclonal anti-FLAG clone M2 (Sigma-Aldrich;

646 1:200), rabbit monoclonal anti-Flag 8H8L17 (ThermoFisher; 1:500), mouse anti-HRP2 clone
647 2G12 (1:500) (97), rabbit polyclonal anti-SBP1 BR28 (1:500) (98) and rabbit polyclonal anti-ACP1
648 (1:500 IFA) (37, 99). Secondary antibodies used were anti-mouse antibody conjugated to Alexa
649 Fluor 488 or 546 and anti-rabbit antibody conjugated to Alexa Fluor 488, (Life Technologies;
650 1:1000). Parasites were mounted with ProLong diamond with 4',6'-diamidino-2-phenylindole
651 (DAPI) (P36931; Invitrogen) and imaged on an Axio Observer 7 equipped with an Axiocam 702
652 mono camera and Zen 2.6 Pro software (Zeiss) using the same exposure times for all images
653 across sample groups and experimental replicates. Image processing, analysis, and display were
654 performed using Zeiss Blue software and Adobe Photoshop. Equivalent adjustments to brightness
655 and contrast were made within sample groups for display purposes.
656
657 **Quantification of protein knockdown.** To evaluate the level of HSP101 protein knockdown,
658 HSP101-kER$^{TetR\text{-}DOZI}$ parasites were synchronized via magnet purification and treated with DMSO
659 or rapamycin before removal of aTc. After aTc removal, parasites were seeded at ~1%
660 parasitemia with different dilutions of aTc and allowed to grow for 48 hrs. Using an Attune NxT
661 flow cytometer, infected RBCs were gated using Hoechst 34580 (Invitrogen; 1:5,000) and mNG
662 fluorescence of infected RBCs was concurrently measured. The same procedure was applied for
663 saponin-released parasites after protease treatment as described above.
664
665 **Western blotting.** Western blotting was performed as described previously (39, 53). Briefly,
666 parasite-infected RBCs were selectively permeabilized by treatment with ice-cold 0.03% saponin
667 in PBS for 15 min followed by lysis with RIPA and centrifugation to remove hemozoin. For
668 constructs expressed from the *attB* locus under control of TetR-DOZI-aptamers, parasites were
669 grown in 500 nM aTc for 24 hrs prior to incubation with DMSO or rapamycin to allow for
670 expression. For the HSP101-kER$^{TetR\text{-}DOZI}$ lines, parasites were treated with DMSO or rapamycin
671 before removal of aTc. After aTc removal, parasites were seeded at ~1% parasitemia with

672 different dilutions of aTc and allowed to grow for 48 hrs before processing. The antibodies used
673 in this study were mouse anti-HA antibody (clone 16B12, BioLegend; 1:500), rabbit polyclonal
674 anti-HA SG77 (ThermoFisher; 1:500), mouse anti-FLAG (Clone M2, Sigma-Aldrich; 1:500), rabbit
675 polyclonal anti-*Plasmodium* Aldolase ab207494 (Abcam; 1:500) and mouse monoclonal anti-
676 EXP2 clone 7.7 (1:500) (100). The secondary antibodies used were IRDye 680CW goat anti-
677 rabbit IgG and IRDye 800CW goat anti-mouse IgG (Li-COR Biosciences; 1:20,000). Western blot
678 images were acquired using an Odyssey Clx infrared imaging system and processed with Image
679 Studio software (Li-COR Biosciences). Full length versions of cropped blots can be seen in Figure
680 S8.
681

682 **Acknowledgements**

683 This work was supported by NIH grant HL133453 to JRB. The funders had no role in study design,
684 data collection and interpretation, or the decision to submit the work for publication. We thank J.
685 McBride, D. Cavanaugh and EMRR for the EXP2 antibody and A. Waters for the HP DiCre *P.*
686 *berghei* parasites.
687

688 **Author contributions**

689 M.A.F. and J.R.B designed research; M.A.F., T.H., L.J.C. and J.R.B performed research; M.A.F.
690 and J.R.B analyzed data; M.A.F. and J.R.B. wrote the paper.

691 **References**

692 1. G. G. van Dooren, B. Striepen, The algal past and parasite present of the apicoplast.
693 *Annu Rev Microbiol* **67**, 271-289 (2013).

694 2. O. A. Akuh, R. Elahi, S. T. Prigge, F. Seeber, The ferredoxin redox system - an essential
695 electron distributing hub in the apicoplast of Apicomplexa. *Trends Parasitol* **38**, 868-881
696 (2022).

697 3. M. M. Cova, M. H. Lamarque, M. Lebrun, How Apicomplexa Parasites Secrete and Build
698 Their Invasion Machinery. *Annu Rev Microbiol* **76**, 619-640 (2022).

699 4. J. M. Matz, J. R. Beck, M. J. Blackman, The parasitophorous vacuole of the blood-stage
700 malaria parasite. *Nat Rev Microbiol* **18**, 379-391 (2020).

701 5. M. Garten, J. R. Beck, Structured to conquer: transport across the Plasmodium
702 parasitophorous vacuole. *Curr Opin Microbiol* **63**, 181-188 (2021).

703 6. T. F. de Koning-Ward, M. W. Dixon, L. Tilley, P. R. Gilson, Plasmodium species: master
704 renovators of their host cells. *Nat Rev Microbiol* **14**, 494-507 (2016).

705 7. J. R. Beck, C. M. Ho, Transport mechanisms at the malaria parasite-host cell interface.
706 *PLoS Pathog* **17**, e1009394 (2021).

707 8. T. J. Sargeant *et al.*, Lineage-specific expansion of proteins exported to erythrocytes in
708 malaria parasites. *Genome Biol* **7**, R12 (2006).

709 9. J. A. Boddey *et al.*, Role of plasmepsin V in export of diverse protein families from the
710 Plasmodium falciparum exportome. *Traffic* **14**, 532-550 (2013).

711 10. C. van Ooij *et al.*, The malaria secretome: from algorithms to essential function in blood
712 stage infection. *PLoS Pathog* **4**, e1000084 (2008).

713 11. J. Schulze *et al.*, The Plasmodium falciparum exportome contains non-canonical
714 PEXEL/HT proteins. *Mol Microbiol* **97**, 301-314 (2015).

715 12. T. K. Jonsdottir, M. Gabriela, B. S. Crabb, T. F. de Koning-Ward, P. R. Gilson, Defining
716 the Essential Exportome of the Malaria Parasite. *Trends Parasitol* **37**, 664-675 (2021).

717 13. A. Florentin, D. W. Cobb, H. M. Kudyba, V. Muralidharan, Directing traffic: Chaperone-
718 mediated protein transport in malaria parasites. *Cell Microbiol* **22**, e13215 (2020).

719 14. S. Munro, H. R. Pelham, A C-terminal signal prevents secretion of luminal ER proteins.
720 *Cell* **48**, 899-907 (1987).

721 15. P. Brauer *et al.*, Structural basis for pH-dependent retrieval of ER proteins from the Golgi
722 by the KDEL receptor. *Science* **363**, 1103-1107 (2019).

723 16. A. Gerondopoulos *et al.*, A signal capture and proofreading mechanism for the KDEL-
724 receptor explains selectivity and dynamic range in ER retrieval. *Elife* **10** (2021).

725 17. H. G. Elmendorf, K. Haldar, Identification and localization of ERD2 in the malaria
726 parasite Plasmodium falciparum: separation from sites of sphingomyelin synthesis and
727 implications for organization of the Golgi. *EMBO J* **12**, 4763-4773 (1993).

728 18. N. La Greca, A. R. Hibbs, C. Riffkin, M. Foley, L. Tilley, Identification of an endoplasmic
729 reticulum-resident calcium-binding protein with multiple EF-hand motifs in asexual
730 stages of Plasmodium falciparum. *Mol Biochem Parasitol* **89**, 283-293 (1997).

731 19. S. Kulzer, N. Gehde, J. M. Przyborski, Return to sender: use of Plasmodium ER retrieval
732 sequences to study protein transport in the infected erythrocyte and predict putative ER
733 protein families. *Parasitol Res* **104**, 1535-1541 (2009).

734 20. H. M. Kudyba *et al.*, The endoplasmic reticulum chaperone PfGRP170 is essential for
735 asexual development and is linked to stress response in malaria parasites. *Cell Microbiol*
736 **21**, e13042 (2019).

737 21. D. W. Cobb *et al.*, A redox-active crosslinker reveals an essential and inhibitable
738 oxidative folding network in the endoplasmic reticulum of malaria parasites. *PLoS*
739 *Pathog* **17**, e1009293 (2021).

740 22. M. A. Fierro *et al.*, An Endoplasmic Reticulum CREC Family Protein Regulates the
741 Egress Proteolytic Cascade in Malaria Parasites. *mBio* **11** (2020).

742 23. J. R. Beck, V. Muralidharan, A. Oksman, D. E. Goldberg, PTEX component HSP101
743 mediates export of diverse malaria effectors into host erythrocytes. *Nature* **511**, 592-595
744 (2014).

745 24. B. Elsworth *et al.*, PTEX is an essential nexus for protein export in malaria parasites.
746 *Nature* **511**, 587-591 (2014).

747 25. C. M. Ho *et al.*, Malaria parasite translocon structure and mechanism of effector export.
748 *Nature* **561**, 70-75 (2018).

749 26. C. R. Collins *et al.*, Robust inducible Cre recombinase activity in the human malaria
750 parasite Plasmodium falciparum enables efficient gene deletion within a single asexual
751 erythrocytic growth cycle. *Mol Microbiol* **88**, 687-701 (2013).

752 27. E. Knuepfer, M. Napiorkowska, C. van Ooij, A. A. Holder, Generating conditional gene
753 knockouts in Plasmodium - a toolkit to produce stable DiCre recombinase-expressing
754 parasite lines using CRISPR/Cas9. *Sci Rep* **7**, 3881 (2017).

755 28. M. L. Jones *et al.*, A versatile strategy for rapid conditional genome engineering using
756 loxP sites in a small synthetic intron in Plasmodium falciparum. *Sci Rep* **6**, 21800 (2016).

757 29. J. M. Przyborski *et al.*, Trafficking of STEVOR to the Maurer's clefts in Plasmodium
758 falciparum-infected erythrocytes. *EMBO J* **24**, 2306-2317 (2005).

759 30. G. G. van Dooren *et al.*, Development of the endoplasmic reticulum, mitochondrion and
760 apicoplast during the asexual life cycle of Plasmodium falciparum. *Mol Microbiol* **57**, 405-
761 419 (2005).

762 31. C. J. Tonkin, N. S. Struck, K. A. Mullin, L. M. Stimmler, G. I. McFadden, Evidence for
763 Golgi-independent transport from the early secretory pathway to the plastid in malaria
764 parasites. *Mol Microbiol* **61**, 614-630 (2006).

765 32. M. C. Lee, P. A. Moura, E. A. Miller, D. A. Fidock, Plasmodium falciparum Sec24 marks
766 transitional ER that exports a model cargo via a diacidic motif. *Mol Microbiol* **68**, 1535-
767 1546 (2008).

768 33. S. R. Heiny, S. Pautz, M. Recker, J. M. Przyborski, Protein Traffic to the Plasmodium
769 falciparum apicoplast: evidence for a sorting branch point at the Golgi. *Traffic* **15**, 1290-
770 1304 (2014).

771 34. J. M. Matz *et al.*, The Plasmodium berghei translocon of exported proteins reveals
772 spatiotemporal dynamics of tubular extensions. *Sci Rep* **5**, 12532 (2015).

773 35. M. J. Boucher *et al.*, Integrative proteomics and bioinformatic prediction enable a high-
774 confidence apicoplast proteome in malaria parasites. *PLoS Biol* **16**, e2005895 (2018).

775 36. J. Birnbaum *et al.*, A Kelch13-defined endocytosis pathway mediates artemisinin
776 resistance in malaria parasites. *Science* **367**, 51-59 (2020).

777 37. R. F. Waller, M. B. Reed, A. F. Cowman, G. I. McFadden, Protein trafficking to the
778 plastid of Plasmodium falciparum is via the secretory pathway. *EMBO J* **19**, 1794-1802
779 (2000).

780 38. A. Adisa *et al.*, The signal sequence of exported protein-1 directs the green fluorescent
781 protein to the parasitophorous vacuole of transfected malaria parasites. *J Biol Chem*
782 **278**, 6532-6542 (2003).

783 39. T. Nessel *et al.*, EXP1 is required for organisation of EXP2 in the intraerythrocytic
784 malaria parasite vacuole. *Cell Microbiol* **22**, e13168 (2020).

785 40. S. M. Ganesan, A. Falla, S. J. Goldfless, A. S. Nasamu, J. C. Niles, Synthetic RNA-
786 protein modules integrated with native translation mechanisms to control gene
787 expression in malaria parasites. *Nat Commun* **7**, 10727 (2016).

788 41. K. Rajaram, H. B. Liu, S. T. Prigge, Redesigned TetR-Aptamer System To Control Gene
789 Expression in Plasmodium falciparum. *mSphere* **5** (2020).

790 42. S. H. Adjalley *et al.*, Quantitative assessment of Plasmodium falciparum sexual
791 development reveals potent transmission-blocking activity by methylene blue. *Proc Natl*
792 *Acad Sci U S A* **108**, E1214-1223 (2011).

793 43. M. El Bakkouri *et al.*, The Clp chaperones and proteases of the human malaria parasite
794 Plasmodium falciparum. *J Mol Biol* **404**, 456-477 (2010).

795 44. E. Yeh, J. L. DeRisi, Chemical rescue of malaria parasites lacking an apicoplast defines
796 organelle function in blood-stage Plasmodium falciparum. *PLoS Biol* **9**, e1001138
797 (2011).

798 45. G. G. van Dooren, V. Su, M. C. D'Ombrain, G. I. McFadden, Processing of an apicoplast
799 leader sequence in Plasmodium falciparum and the identification of a putative leader
800 cleavage enzyme. *J Biol Chem* **277**, 23612-23619 (2002).

801 46. M. Zhang *et al.*, Uncovering the essential genes of the human malaria parasite
802 Plasmodium falciparum by saturation mutagenesis. *Science* **360** (2018).

803 47. E. Bushell *et al.*, Functional Profiling of a Plasmodium Genome Reveals an Abundance
804 of Essential Genes. *Cell* **170**, 260-272 e268 (2017).

805 48. M. E. Fichera, D. S. Roos, A plastid organelle as a drug target in apicomplexan
806 parasites. *Nature* **390**, 407-409 (1997).

807 49. E. L. Dahl, P. J. Rosenthal, Multiple antibiotics exert delayed effects against the
808 Plasmodium falciparum apicoplast. *Antimicrob Agents Chemother* **51**, 3485-3490 (2007).

809 50. N. I. Proellocks *et al.*, Characterisation of PfRON6, a Plasmodium falciparum rhoptry
810 neck protein with a novel cysteine-rich domain. *Int J Parasitol* **39**, 683-692 (2009).

811 51. S. A. Desai, D. J. Krogstad, E. W. McCleskey, A nutrient-permeable channel on the
812 intraerythrocytic malaria parasite. *Nature* **362**, 643-646 (1993).

813 52. S. A. Desai, R. L. Rosenberg, Pore size of the malaria parasite's nutrient channel. *Proc*
814 *Natl Acad Sci U S A* **94**, 2045-2049 (1997).

815 53. M. Garten *et al.*, EXP2 is a nutrient-permeable channel in the vacuolar membrane of
816 Plasmodium and is essential for protein export via PTEX. *Nat Microbiol* **3**, 1090-1098
817 (2018).

818 54. D. A. Gold *et al.*, The Toxoplasma Dense Granule Proteins GRA17 and GRA23 Mediate
819 the Movement of Small Molecules between the Host and the Parasitophorous Vacuole.
820 *Cell Host Microbe* **17**, 642-652 (2015).

821 55. P. R. Sanders *et al.*, The N-terminus of EXP2 forms the membrane-associated pore of
822 the protein exporting translocon PTEX in Plasmodium falciparum. *J Biochem* **165**, 239-
823 248 (2019).

824 56. K. Hakamada, H. Watanabe, R. Kawano, K. Noguchi, M. Yohda, Expression and
825 characterization of the Plasmodium translocon of the exported proteins component
826 EXP2. *Biochem Biophys Res Commun* **482**, 700-705 (2017).

827 57. M. Dal Peraro, F. G. van der Goot, Pore-forming toxins: ancient, but never really out of
828 fashion. *Nat Rev Microbiol* **14**, 77-92 (2016).

829 58. S. C. Charnaud, R. Kumarasingha, H. E. Bullen, B. S. Crabb, P. R. Gilson, Knockdown
830 of the translocon protein EXP2 in Plasmodium falciparum reduces growth and protein
831 export. *PLoS One* **13**, e0204785 (2018).

832 59. P. Mesen-Ramirez *et al.*, EXP1 is critical for nutrient uptake across the parasitophorous
833 vacuole membrane of malaria parasites. *PLoS Biol* **17**, e3000473 (2019).

834 60. T. F. de Koning-Ward *et al.*, A newly discovered protein export machine in malaria
835 parasites. *Nature* **459**, 945-949 (2009).

836 61. M. Gabriela *et al.*, A revised mechanism for how Plasmodium falciparum recruits and
837 exports proteins into its erythrocytic host cell. *PLoS Pathog* **18**, e1009977 (2022).

838 62. S. C. Charnaud *et al.*, Spatial organization of protein export in malaria parasite blood
839 stages. *Traffic* **19**, 605-623 (2018).

840 63. A. Ingmundson, C. Nahar, V. Brinkmann, M. J. Lehmann, K. Matuschewski, The
841 exported Plasmodium berghei protein IBIS1 delineates membranous structures in
842 infected red blood cells. *Mol Microbiol* **83**, 1229-1243 (2012).

843 64. S. Nair *et al.*, Nutrient Limitation Magnifies Fitness Costs of Antimalarial Drug
844 Resistance Mutations. *Antimicrob Agents Chemother* **66**, e0152921 (2022).

845 65. A. Gupta *et al.*, Complex nutrient channel phenotypes despite Mendelian inheritance in a
846 Plasmodium falciparum genetic cross. *PLoS Pathog* **16**, e1008363 (2020).

847 66. J. M. Matz *et al.*, In Vivo Function of PTEX88 in Malaria Parasite Sequestration and
848 Virulence. *Eukaryot Cell* **14**, 528-534 (2015).

849 67. S. A. Chisholm *et al.*, Contrasting Inducible Knockdown of the Auxiliary PTEX
850 Component PTEX88 in P. falciparum and P. berghei Unmasks a Role in Parasite
851 Virulence. *PLoS One* **11**, e0149296 (2016).

852 68. H. M. Kudyba, D. W. Cobb, J. Vega-Rodriguez, V. Muralidharan, Some conditions apply:
853 Systems for studying Plasmodium falciparum protein function. *PLoS Pathog* **17**,
854 e1009442 (2021).

855 69. J. Birnbaum *et al.*, A genetic system to study Plasmodium falciparum protein function.
856 *Nat Methods* **14**, 450-456 (2017).

857 70. K. R. Hughes, A. P. Waters, Rapid inducible protein displacement in. *Wellcome Open*
858 *Res* **2**, 18 (2017).

859 71. A. D. Roberts, S. C. Nair, A. J. Guerra, S. T. Prigge, Development of a conditional
860 localization approach to control apicoplast protein trafficking in malaria parasites. *Traffic*
861 **20**, 571-582 (2019).

862 72. A. Praznik *et al.*, Regulation of protein secretion through chemical regulation of
863 endoplasmic reticulum retention signal cleavage. *Nat Commun* **13**, 1323 (2022).

864 73. A. Prasad, P. Mastud, S. Patankar, Dually localised proteins found in both the apicoplast
865 and mitochondrion utilize the Golgi-dependent pathway for apicoplast targeting in
866 Toxoplasma gondii. *Biol Cell* **113**, 58-78 (2021).

867 74. A. Florentin *et al.*, PfClpC Is an Essential Clp Chaperone Required for Plastid Integrity
868 and Clp Protease Stability in Plasmodium falciparum. *Cell Rep* **21**, 1746-1756 (2017).

869 75. A. Florentin, D. R. Stephens, C. F. Brooks, R. P. Baptista, V. Muralidharan, Plastid
870 biogenesis in malaria parasites requires the interactions and catalytic activity of the Clp
871 proteolytic system. *Proc Natl Acad Sci U S A* **117**, 13719-13729 (2020).

872 76. A. Mogk, B. Bukau, H. H. Kampinga, Cellular Handling of Protein Aggregates by
873 Disaggregation Machines. *Mol Cell* **69**, 214-226 (2018).

874 77. I. Bouchnak, K. J. van Wijk, Structure, function, and substrates of Clp AAA+ protease
875 systems in cyanobacteria, plastids, and apicoplasts: A comparative analysis. *J Biol*
876 *Chem* **296**, 100338 (2021).

877 78. K. Pakos-Zebrucka *et al.*, The integrated stress response. *EMBO Rep* **17**, 1374-1395
878 (2016).

879 79. M. Costa-Mattioli, P. Walter, The integrated stress response: From mechanism to
880 disease. *Science* **368** (2020).

881 80. S. Chaubey, M. Grover, U. Tatu, Endoplasmic reticulum stress triggers
882 gametocytogenesis in the malaria parasite. *J Biol Chem* **289**, 16662-16674 (2014).

883 81. M. B. Harbut *et al.*, Targeting the ERAD pathway via inhibition of signal peptide
884 peptidase for antiparasitic therapeutic design. *Proc Natl Acad Sci U S A* **109**, 21486-
885 21491 (2012).

886 82. M. Zhang *et al.*, PK4, a eukaryotic initiation factor 2alpha(eIF2alpha) kinase, is essential
887 for the development of the erythrocytic cycle of Plasmodium. *Proc Natl Acad Sci U S A*
888 **109**, 3956-3961 (2012).

889 83. M. Zhang *et al.*, Inhibiting the Plasmodium eIF2alpha Kinase PK4 Prevents Artemisinin-
890 Induced Latency. *Cell Host Microbe* **22**, 766-776 e764 (2017).

891 84. Y. S. Levray *et al.*, Formation of ER-lumenal intermediates during export of Plasmodium
892 proteins containing transmembrane-like hydrophobic sequences. *PLoS Pathog* **19**,
893 e1011281 (2023).

894 85. E. C. Gaynor, S. te Heesen, T. R. Graham, M. Aebi, S. D. Emr, Signal-mediated retrieval
895 of a membrane protein from the Golgi to the ER in yeast. *J Cell Biol* **127**, 653-665
896 (1994).

897 86. M. Stornaiuolo *et al.*, KDEL and KKXX retrieval signals appended to the same reporter
898 protein determine different trafficking between endoplasmic reticulum, intermediate
899 compartment, and Golgi complex. *Mol Biol Cell* **14**, 889-902 (2003).

900 87. B. L. Tang, S. H. Wong, S. H. Low, W. J. Hong, Retention of a Type-Ii Surface-
901 Membrane Protein in the Endoplasmic-Reticulum by the Lys-Asp-Glu-Leu Sequence.
902 *Journal of Biological Chemistry* **267**, 7072-7076 (1992).

903 88. B. E. Sleebs *et al.*, Inhibition of Plasmepsin V activity demonstrates its essential role in
904 protein export, PfEMP1 display, and survival of malaria parasites. *PLoS Biol* **12**,
905 e1001897 (2014).

906 89. A. J. Polino, A. S. Nasamu, J. C. Niles, D. E. Goldberg, Assessment of Biological Role
907 and Insight into Druggability of the Plasmodium falciparum Protease Plasmepsin V. *ACS*
908 *Infect Dis* **6**, 738-746 (2020).

909 90. S. H. Adjalley, M. C. S. Lee, D. A. Fidock, "A Method for Rapid Genetic Integration into
910 Plasmodium falciparum Utilizing Mycobacteriophage Bxb1 Integrase". (Humana Press,
911 2010), 10.1007/978-1-60761-652-8_6, pp. 87-100.

912 91. S. Glushakova *et al.*, Exploitation of a newly-identified entry pathway into the malaria
913 parasite-infected erythrocyte to inhibit parasite egress. *Sci Rep* **7**, 12250 (2017).

914 92. A. I. Ahiya, S. Bhatnagar, J. M. Morrisey, J. R. Beck, A. B. Vaidya, Dramatic
915 Consequences of Reducing Erythrocyte Membrane Cholesterol on Plasmodium
916 falciparum. *Microbiol Spectr* **10**, e0015822 (2022).

917 93. T. W. Kooij, M. M. Rauch, K. Matuschewski, Expansion of experimental genetics
918 approaches for Plasmodium berghei with versatile transfection vectors. *Mol Biochem*
919 *Parasitol* **185**, 19-26 (2012).

920 94. C. J. Janse, J. Ramesar, A. P. Waters, High-efficiency transfection and drug selection of
921 genetically transformed blood stages of the rodent malaria parasite Plasmodium berghei.
922 *Nat Protoc* **1**, 346-356 (2006).

923 95. R. S. Kent *et al.*, Inducible developmental reprogramming redefines commitment to
924 sexual development in the malaria parasite Plasmodium berghei. *Nat Microbiol* **3**, 1206-
925 1213 (2018).

926 96. J. Schindelin *et al.*, Fiji: an open-source platform for biological-image analysis. *Nat*
927 *Methods* **9**, 676-682 (2012).

928 97. E. P. Rock *et al.*, Comparative analysis of the Plasmodium falciparum histidine-rich
929 proteins HRP-I, HRP-II and HRP-III in malaria parasites of diverse origin. *Parasitology*
930 **95 (Pt 2)**, 209-227 (1987).

931 98. T. Blisnick *et al.*, Pfsbp1, a Maurer's cleft Plasmodium falciparum protein, is associated
932 with the erythrocyte skeleton. *Mol Biochem Parasitol* **111**, 107-121 (2000).

933 99. M. Ponpuak *et al.*, A role for falcilysin in transit peptide degradation in the Plasmodium
934 falciparum apicoplast. *Mol Microbiol* **63**, 314-334 (2007).

935 100. R. Hall *et al.*, Antigens of the Erythrocytic Stages of the Human Malaria Parasite
936 Plasmodium-Falciparum Detected by Monoclonal-Antibodies. *Molecular and*
937 *Biochemical Parasitology* **7**, 247-265 (1983).

938 101. K. Matthews *et al.*, The Plasmodium translocon of exported proteins (PTEX) component
939 thioredoxin-2 is important for maintaining normal blood-stage growth. *Mol Microbiol* **89**,
940 1167-1186 (2013).

941

942

943 **Figures**

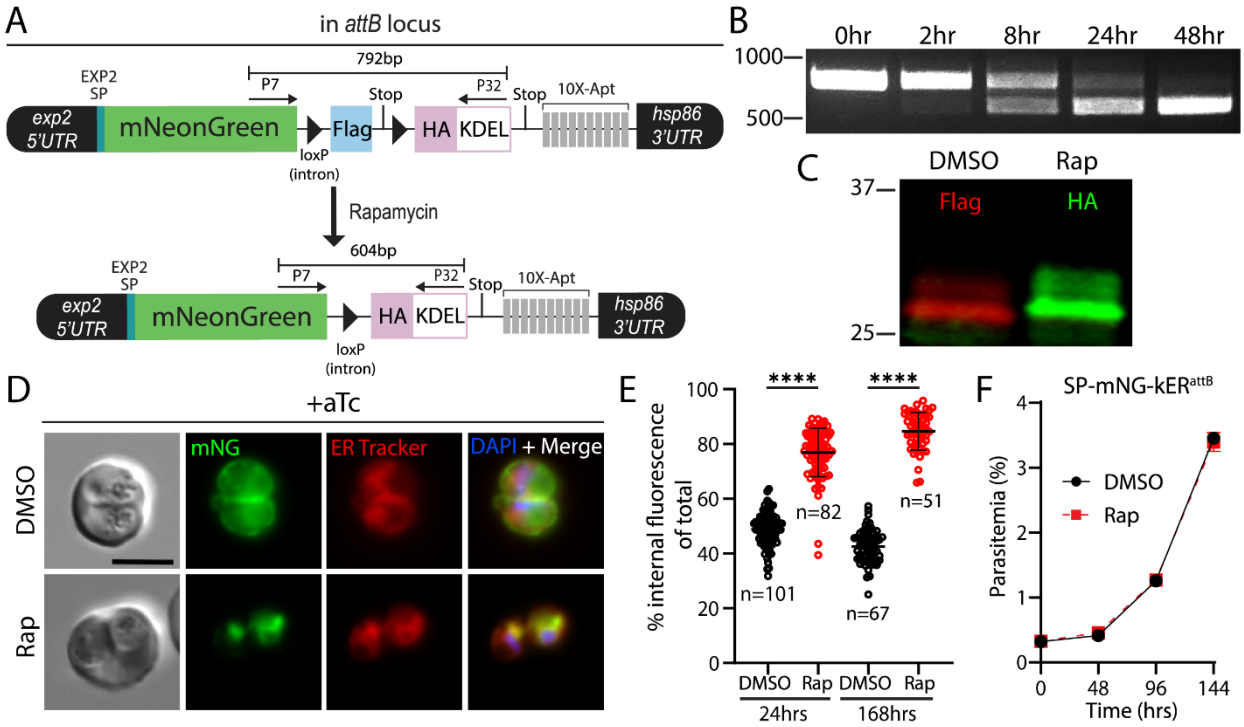

944 **Figure 1. Conditional ER retrieval of a secreted reporter does not impact parasite fitness.**
945 A) Schematic of reporter expression cassette installed at the *attB* site of chromosome 6. An
946 mNeonGreen reporter is fused to the signal peptide of EXP2 and expressed under control of the
947 *exp2* promoter. A 3xFLAG tag and stop codon are flanked by loxP-containing introns (triangles)
948 followed by a 3xHA-KDEL, stop codon, and 10X aptamer array (10X-Apt). Aptamer interaction
949 with TetR-DOZI (expressed from a cassette in the plasmid not shown) prevents translation of the
950 reporter, which is relieved in the presence of anhydrotetracycline (aTc) to enable expression.
951 Activation of DiCre by rapamycin treatment excises the FLAG tag, bringing into frame the HA-
952 KDEL tag. B) Time course of excision following rapamycin treatment detected by PCR using
953 primers P7/32. C) Western blot of mNG reporter 24hrs post treatment with DMSO or rapamycin.
954 Molecular weights after signal peptide cleavage are predicted to be 30.8 kDa for mNG-3xFLAG
955 and 30.9 kDa for mNG-3xHA-KDEL. D) Live microscopy of DMSO or rapamycin-treated parasites
956 24hrs post-treatment. E) Quantification of percent internal mNG fluorescence 24hrs and 168hrs
957 post-treatment with DMSO or rapamycin. Data are pooled from 2 independent experiments and

958 bar indicates mean (****, P<0.0001; unpaired t test). F) Representative growth of asynchronous
959 parasites (n=2 biological replicates) treated with DMSO or rapamycin. Data are presented as
960 means ± standard deviation from one biological replicate (n = 3 technical replicates). All cultures
961 were maintained in media supplemented with 500 nM aTc. Scale bar, 5μm.

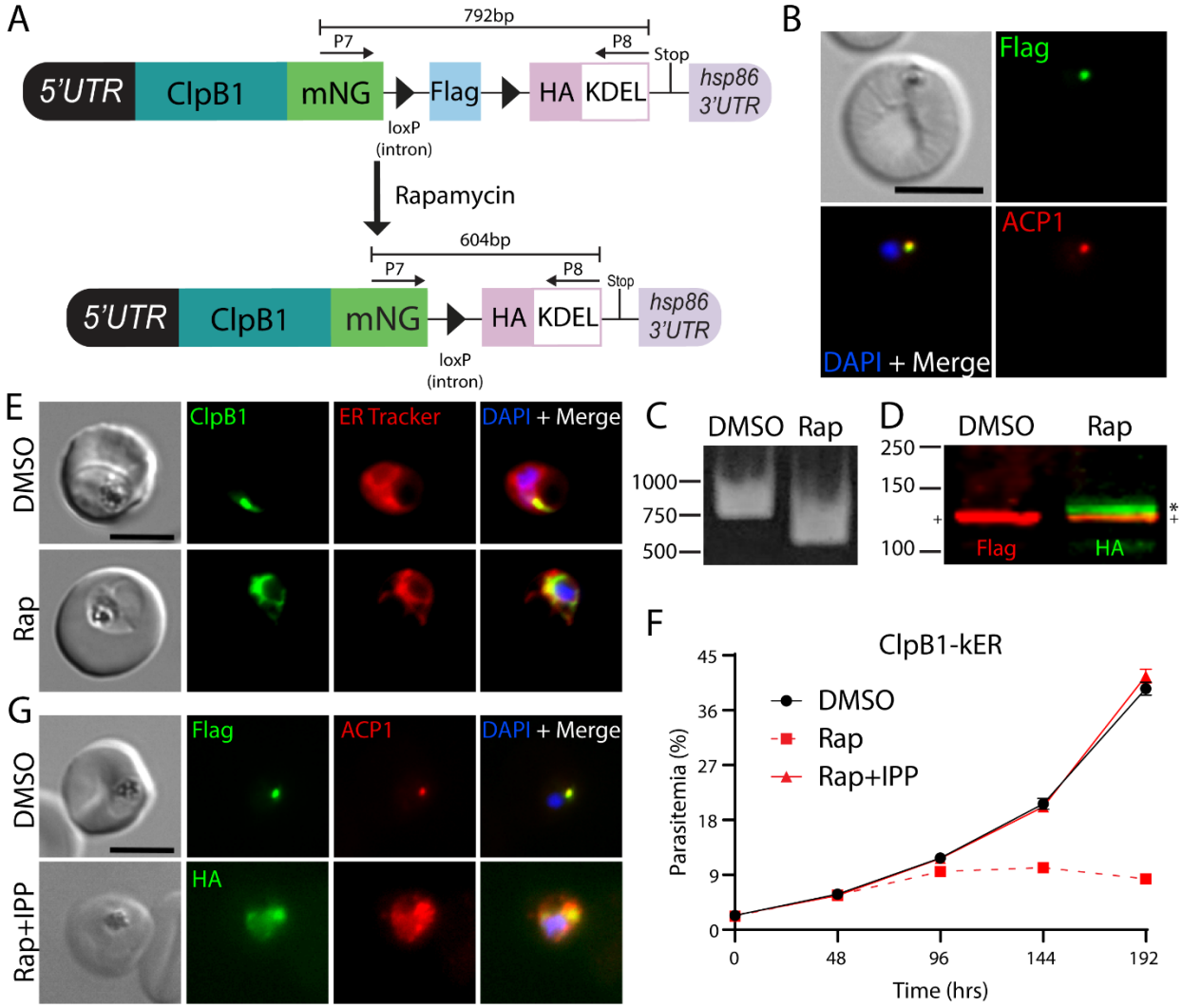

Figure 2. Lethal ER retention of the apicoplast chaperone ClpB1 is rescued by IPP. A) Schematic showing strategy for appending kER to the C-terminus of *clpB1*. B) IFA of PFA fixed parasites stained with mouse anti-Flag and rabbit anti-ACP1 antibodies. C) PCR showing excision in ClpB1-kER parasites 24hrs after rapamycin treatment using primers P7/8. D) Western blot 24hrs post treatment with DMSO or rapamycin. Molecular weights after transit peptide cleavage are predicted to be 135 kDa for ClpB1-mNG-3xFLAG and 135.1 kDa for ClpB1-mNG-3xHA-KDEL. (+) represents the mature form of ClpB1 while the (*) represents ClpB1 with the transit peptide still attached. E) Live microscopy of DMSO or rapamycin-treated parasites 48hrs post-treatment. F) Representative growth of asynchronous parasites (n=3 biological replicates) treated with DMSO or rapamycin, with or without supplementation with 200 μM IPP. Data are presented as

972 means ± standard deviation from one biological replicate (n = 3 technical replicates). G) IFA of
973 PFA fixed parasites stained with mouse anti-Flag or anti-HA and rabbit anti-ACP1 antibodies after
974 3 growth cycles where rapamycin treated parasites were supplemented with 200 μM IPP. Scale
975 bars, 5μm.

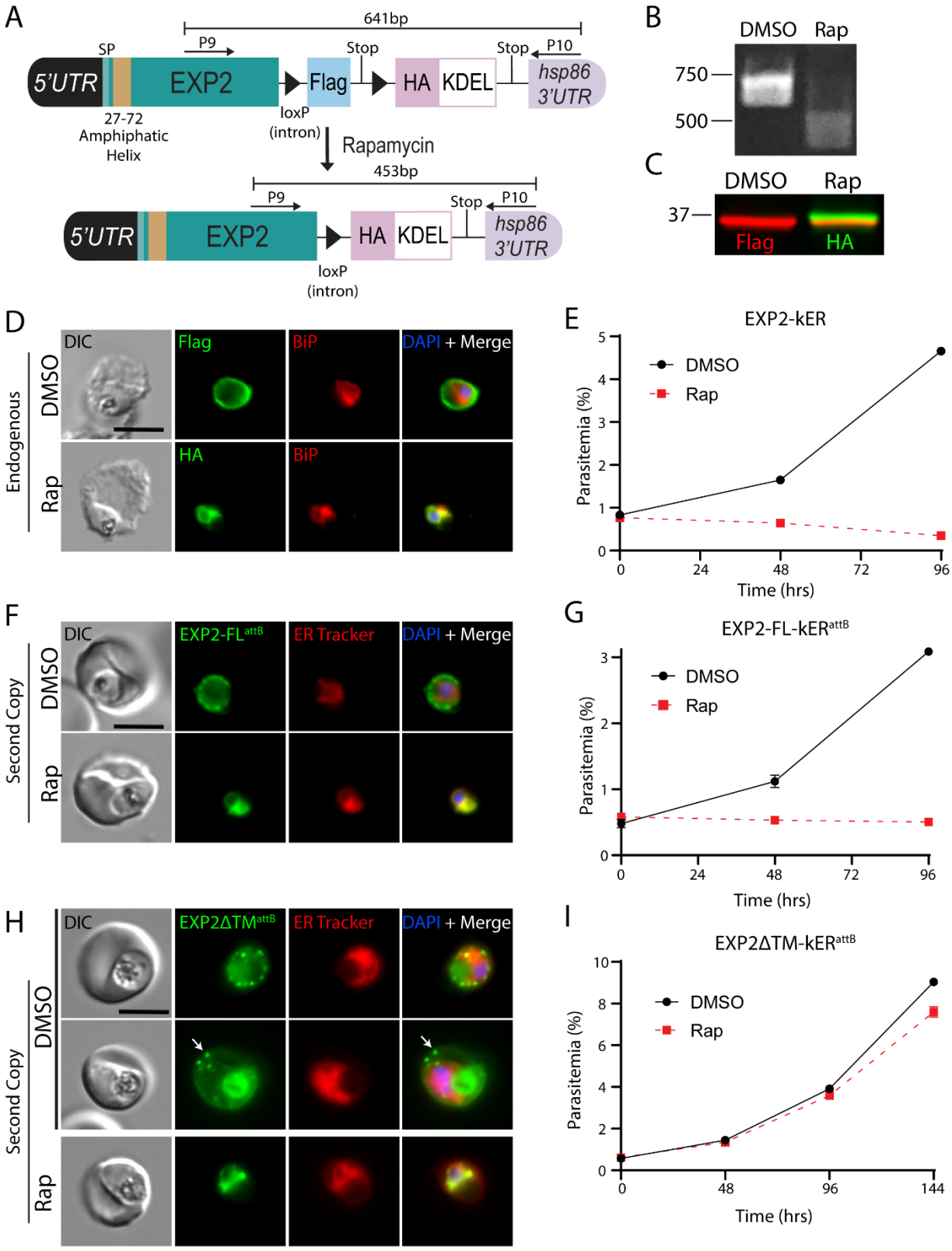

976 **Figure 3. ER retention of EXP2 causes a lethal fitness defect independent of loss of PVM**

977 **transport functions.** A) Schematic showing strategy for appending kER to the endogenous C-

978 terminus of EXP2 without mNG. B) PCR showing excision in EXP2-kER 24hrs after treatment
979 with rapamycin using primers P9/10. C) Western blot of EXP2-kER parasites 24hrs post treatment
980 with DMSO or rapamycin. Molecular weights after signal peptide cleavage are predicted to be
981 34.6 kDa for EXP2-3xFLAG and 34.7 kDa for EXP2-3xHA-KDEL. D) IFA of EXP2-kER 24hrs post-
982 treatment with DMSO or rapamycin. E) Growth of asynchronous parasites (n=2 biological
983 replicates) treated with DMSO or rapamycin. Data are presented as means ± standard deviation
984 from one biological replicate (n = 3 technical replicates). F) Live microscopy of parasites
985 expressing a full-length second copy of EXP2 with an mNG-kER fusion from the *attB* site under
986 the control of the endogenous *exp2* promoter (EXP2-FL-kER^{attB}). Parasites were viewed 24hrs
987 after treatment with DMSO or rapamycin. G) Representative growth of asynchronous EXP2-FL-
988 kER^{attB} parasites (n=2 biological replicates) treated with DMSO or rapamycin. Data are presented
989 as means ± standard deviation from one biological replicate (n = 3 technical replicates). H) Live
990 microscopy of parasites expressing a second copy of EXP2 with mNG-kER fusion and lacking
991 the amphipathic helix from the *attB* site (EXP2ΔTM-kER^{attB}). Parasites were viewed 24hrs after
992 treatment with DMSO or rapamycin. Two representative examples of unexcised parasites are
993 presented, showing localization of the ΔTM version of EXP2 to the PV and host cell in some
994 infected RBCs (arrow). Digestive vacuole fluorescence was also observed as is typical for PV
995 proteins. I) Representative growth of asynchronous EXP2ΔTM-kER^{attB} parasites (n=2 biological
996 replicates) treated with DMSO or rapamycin. Data are presented as means ± standard deviation
997 from one biological replicate (n = 3 technical replicates). Second copy EXP2-kER lines were
998 maintained in media supplemented with 500 nM aTc. Scale bars, 5μm.

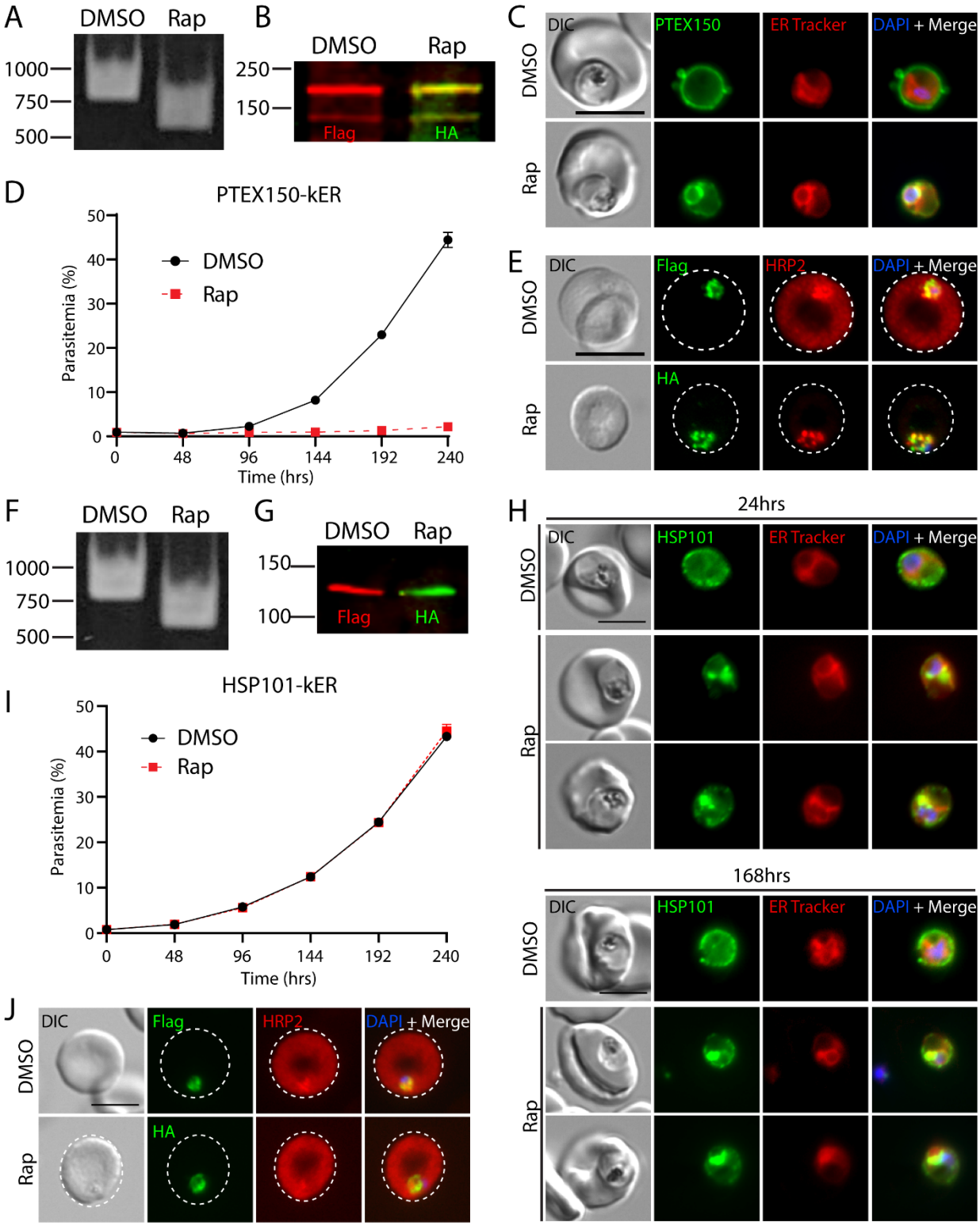

999 **Figure 4. ER retention of PTEX150 but not HSP101 causes a lethal block in protein export**

1000 **in *P. falciparum*.** A) PCR showing excision in PTEX150-kER parasites 24hrs after rapamycin

1001 treatment using primers P7/8. B) Western blot of PTEX150-kER 24hrs post-treatment with DMSO

1002 or rapamycin. Molecular weights after signal peptide cleavage are predicted to be 141 kDa for
1003 PTEX150-mNG-3xFLAG and 141.1 kDa for PTEX150-mNG-3xHA-KDEL. Note that PTEX150 is
1004 observed to migrate at higher molecular weight than predicted (60). C) Live microscopy of
1005 PTEX150-kER 24hrs post-treatment with DMSO or rapamycin. D) Representative growth of
1006 asynchronous PTEX150-kER parasites (n=3 biological replicates) treated with DMSO or
1007 rapamycin. Data are presented as means ± standard deviation from one biological replicate (n = 3
1008 technical replicates). E) IFA of synchronized, ring-stage PTEX150-kER parasites 48hrs post-
1009 treatment with DMSO or rapamycin and probed with anti-HRP2 and anti-FLAG or anti-HA
1010 antibodies. F) PCR showing excision in HSP101-kER parasites 24hrs after rapamycin treatment
1011 using primers P7/8. G) Western blot of HSP101-kER parasites 14 days post-treatment with DMSO
1012 or rapamycin. Molecular weights after signal peptide cleavage are predicted to be 130.5 kDa for
1013 HSP101-mNG-3xFLAG and 130.6 kDa for HSP101-mNG-3xHA-KDEL. H) Live microscopy of
1014 HSP101-kER 24hrs and 168hrs post-treatment with DMSO or rapamycin. I) Representative
1015 growth of asynchronous HSP101-kER parasites (n=3 biological replicates) treated with DMSO or
1016 rapamycin. Data are presented as means ± standard deviation from one biological replicate (n = 3
1017 technical replicates). J) IFA of synchronized, ring-stage HSP101-kER parasites 48hrs post-
1018 treatment with DMSO or rapamycin and probed with anti-HRP2 and anti-FLAG or anti-HA
1019 antibodies. Scale bar, 5μm.

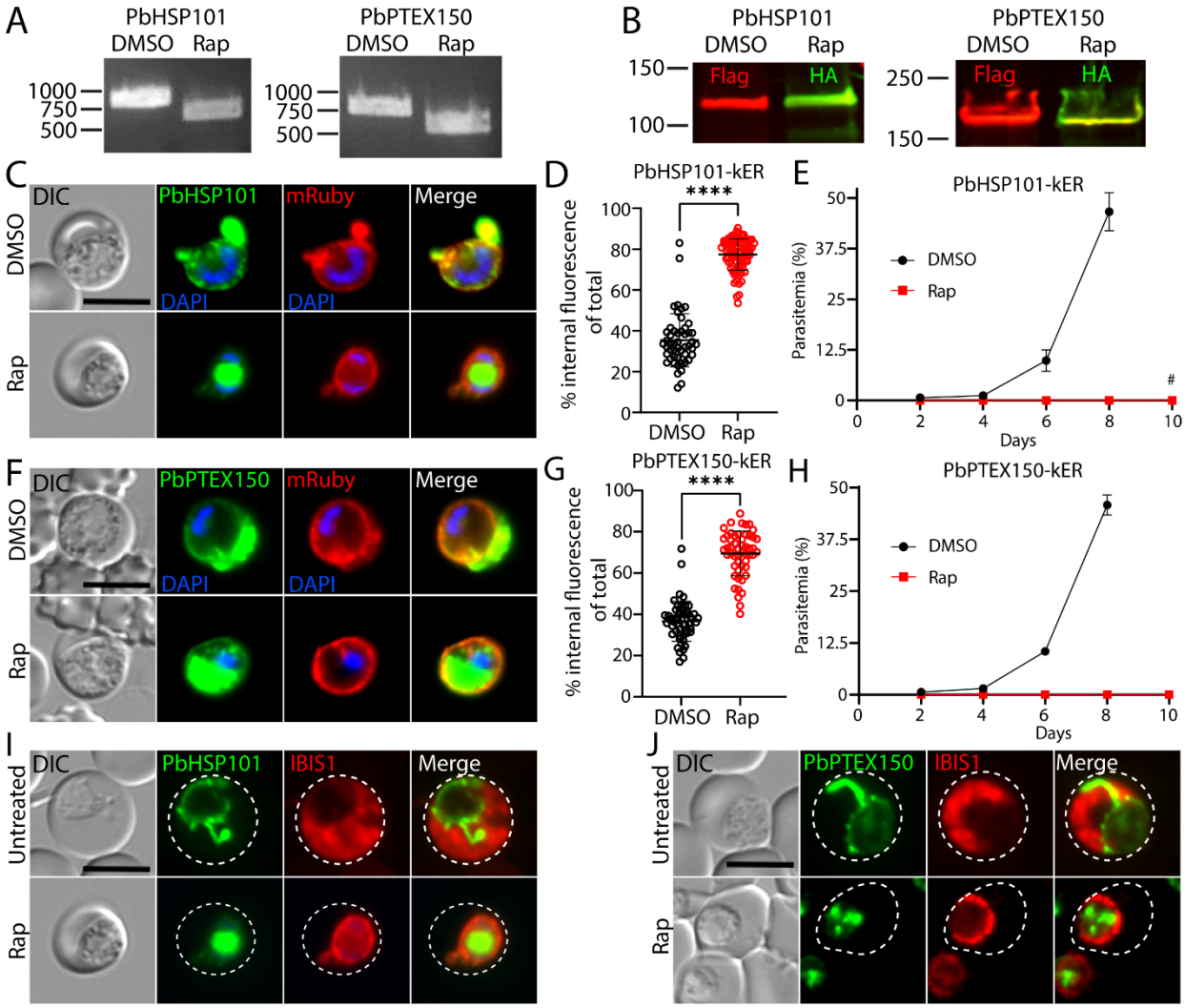

Figure 5: ER retention of HSP101 causes a lethal block in protein export in *P. berghei*. A) PCR showing excision in PbPTEX150-kER and PbHSP101-kER *P. berghei* parasites treated with rapamycin and cultured 18hrs *ex vivo* using primers P7/P60. B) Western blot of PbPTEX150-kER and PbHSP101-kER parasites 24hrs post-treatment with DMSO or rapamycin. Molecular weights after signal peptide cleavage are predicted to be 130.9 kDa for PbHSP101-mNG-3xFLAG, 131 kDa for PbHSP101-mNG-3xHA-KDEL, 130.5 kDa for PbPTEX150-mNG-3xFLAG and 130.6 kDa for PbPTEX150-mNG-3xHA-KDEL. Note that PbPTEX150 is observed to migrate at higher molecular weight than predicted (101). C,F) Live microscopy of PbHSP101-kER or PbPTEX150-kER parasites 18hrs post-treatment with DMSO or rapamycin. These transgenic lines also contain a downstream cassette for expression of mRuby bearing a signal peptide for secretion into the

1030 PV (see Figure S6A). D,G) Quantification of percent internal mNG fluorescence 24hrs post-
1031 treatment with DMSO or rapamycin. Data are pooled from 2 independent experiments and bar
1032 indicates mean (****, P<0.0001; unpaired t test). E,H) Parasitemia of PbHSP101-kER or
1033 PbPTEX150-kER infected mice inoculated by tail vein-injection of parasites treated *ex vivo* with
1034 DMSO or rapamycin. Data are presented as means ± standard deviation of three independent
1035 experiments (one mouse infected per treatment in each experiment). No parasites were observed
1036 in mice injected with rapamycin treated parasites except that one mouse injected with rapamycin-
1037 treated PbHSP101-kER parasites became patent on day 10 (#). However, PCR showed these
1038 parasites had not undergone excision (see Figure S6B). I,J) Live microscopy of PbHSP101-kER
1039 or PbPTEX150-kER parasites containing a downstream cassette for expression of an IBIS1-
1040 mRuby fusion that is exported into the RBC (See Figure S6A). Parasites were imaged before or
1041 24hrs after treatment with rapamycin. Dashed lines indicate RBC boundaries traced from DIC
1042 images. Images are representative of n=2 biological replicates. Scale bars, 5μm.

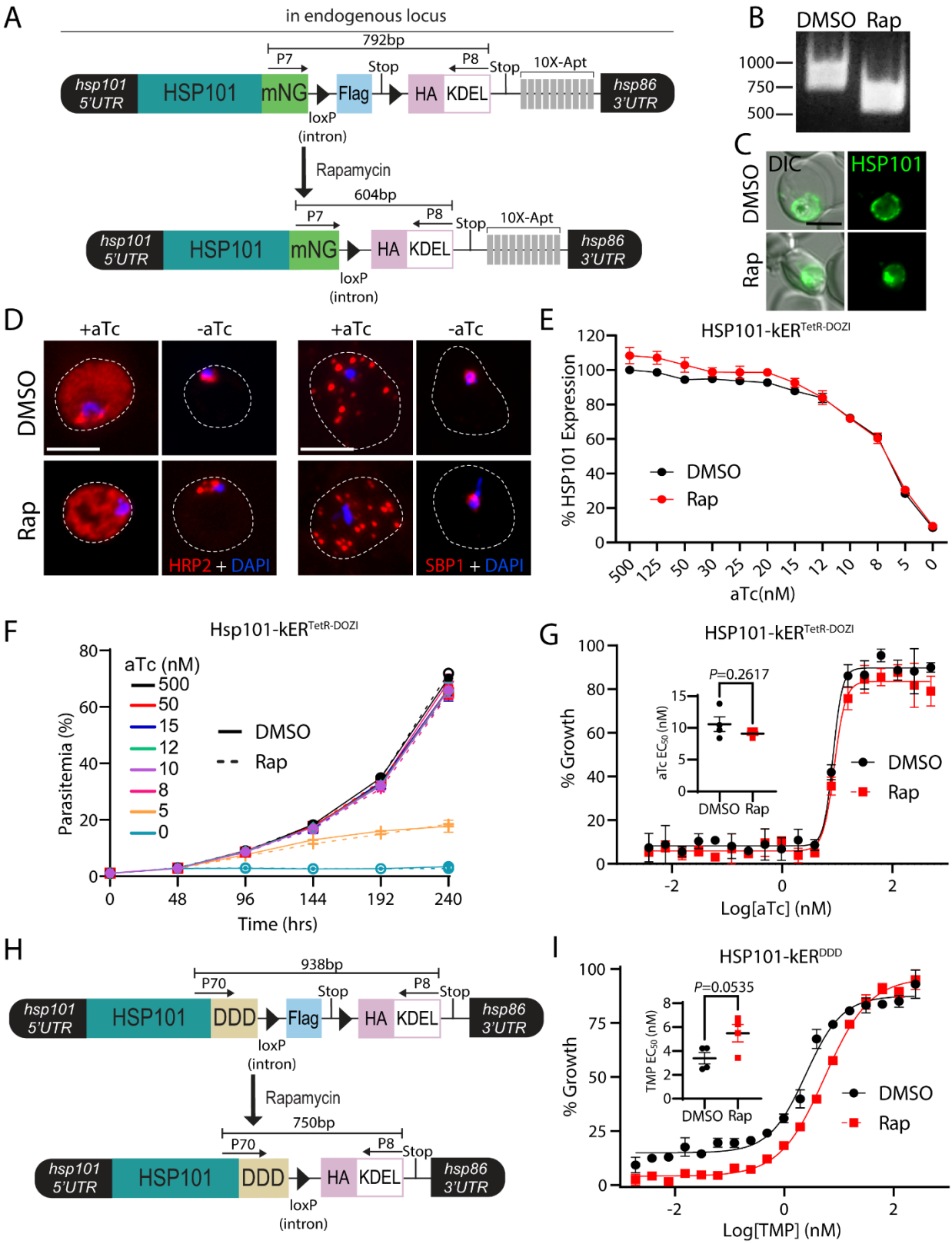

1043 **Figure 6. Depletion of HSP101 PV levels hypersensitizes parasites to post-translational**

1044 **destabilization of the HSP101-PTEX complex but not HSP101 translational knockdown.** A)

1045 Schematic showing strategy for appending kER and the TetR-DOZI aptamers system to the
1046 endogenous C-terminus of HSP101. B) PCR showing excision in HSP101-kER$^{TetR-DOZI}$ parasites
1047 24hrs after rapamycin treatment using primers P7/8. C) Live microscopy of HSP101-kER$^{TetR-DOZI}$
1048 parasites 168hrs post-treatment with DMSO or rapamycin. D) IFA detecting the soluble PEXEL
1049 protein HRP2 or the transmembrane PNEP SBP1 in synchronized, ring-stage HSP101-kER^{TetR-}
1050 ^{DOZI} parasites grown for 48hrs +/- aTc and treated with DMSO or rapamycin 1 cycle prior. Dashed
1051 lines indicate RBC boundaries traced from DIC images. E) Quantification of HSP101 levels by
1052 flow cytometry measurement of mNeonGreen fluorescence in HSP101-kER$^{TetR-DOZI}$ parasites
1053 grown for 48 hrs at indicated aTc concentrations and treated with DMSO or rapamycin 2 cycles
1054 prior. MFI data were normalized to DMSO-treated parasites grown in 500 nM aTc (100%) and
1055 presented as mean ± SEM (n = 5 biological replicates). F) Representative growth curves (n = 4
1056 biological replicates) of HSP101-kER$^{TetR-DOZI}$ parasites grown at indicated aTc concentrations and
1057 treated with DMSO or rapamycin 2 cycles prior. Data are presented as means ± standard
1058 deviation from one biological replicate (n = 3 technical replicates). G) Representative EC_{50} assays
1059 (n=4 biological replicates) with two-fold dilutions of aTc starting at 500nM. Parasites were treated
1060 with DMSO or rapamycin 72 hours prior to adjusting aTc concentrations. Data are presented as
1061 means ± standard deviation from one biological replicate (n = 3 technical replicates). EC_{50} graph
1062 inset presented as mean ± SEM (n = 4 biological replicates): DMSO=10.58±1.16 nM and
1063 rapamycin=9.11±0.29 nM. H) Schematic showing strategy for appending kER and the DDD
1064 system to the endogenous C-terminus of HSP101. I) Representative EC_{50} assays (n=4 biological
1065 replicates) with two-fold dilutions of TMP starting at 250nM. Parasites were treated with DMSO
1066 or rapamycin 72 hours prior to adjusting TMP concentrations. Data are presented as means ±
1067 standard deviation from one biological replicate (n = 3 technical replicates). EC_{50} graph inset
1068 presented as mean ± SEM (n = 4 biological replicates): DMSO=3.39±0.48 nM and rapamycin
1069 5.48±0.73 nM. Scale bars, 5μm.